ISBN 82-553-0680-3 No 2
October 1989

Wave forces on three-dimensional floating bodies with small forward speed

by

Jan Nossen, Enok Palm and John Grue

Wave forces on three-dimensional floating bodies with small forward speed

Jan Nossen, Enok Palm and John Grue

University of Oslo
October 1989

Abstract

The main objective of this report is to describe how to compute wave drift forces and wave drift damping for marine structures of arbitrary three-dimensional shape.

A boundary integral method is developed for computing first-order and mean second-order wave forces on floating bodies with small forward speed in three dimensions. The method is based on applying Green's theorem and linearizing the Green function and velocity potential in the forward speed. The velocity potential on the wetted body surface is then given as the solution of two sets of integral equations with unknowns only on the body. The equations contain no waterline integral, and the free surface integral decays rapidly.

The Timman-Newman relations for the added mass and damping are derived for the case when the double-body flow around the body is included in the free surface condition. The mean drift force is found by far-field analysis. A far-field form of the Haskind relations with forward speed is also derived. All the derivations are made for an arbitrary wave heading.

A boundary element program utilizing the new method has been developed. Numerical results and convergence tests are presented for several body geometries. It is found that interference phenomena may lead to negative wave drift damping for bodies of complicated shape. The results are compared to those of Zhao and Faltinsen (1989), with quite good agreement.

Contents

Chapter 1

Introduction

An important problem in offshore technology is the slow drift motions of floating marine structures. Large horizontal excursions of oil platforms and drilling ships may lead to critical loads on the mooring systems. The slow drift motions are excited by nonlinear wave forces. Damping of the slow-drift oscillations is provided by skin friction, viscous pressure forces and wave drift damping. Since experiments are expensive and time consuming, it is important to be able to predict the wave drift forces theoretically. In this paper, we will present a new method to compute first-order unsteady forces and wave drift forces at small forward speed. Numerical results are shown for a variety of geometries.

The viscous forces are neglected, under the assumption that inertial and viscous effects may be separated. We are not concerned with wave resistance or steady viscous drag, but viscous effects resulting from separation of the boundary layer may still have appreciable effect on the wave forces. It is assumed that these effects are small when the body is large compared to the wave amplitude. Consequently the fluid is assumed irrotational and incompressible. Potential theory is used, and the boundary conditions are linearized with respect to the incident-wave amplitude.

We still have a nonlinear boundary value problem, as long as no restrictions are made upon the body shape or the Froude number. The steady part of the velocity potential, corresponding to the disturbance imposed on the uniform current by the body, satisfies a nonlinear free surface condition, except for deeply submerged bodies.

In ship hydrodynamics, this difficulty is often overcome by assuming that the body is thin or slender, so it only makes a slight disturbance of the steady flow. A perturbation expansion with respect to a slenderness parameter is then used. We are, however, interested in finding the responses of more generally shaped bodies, such as oil platforms, storage tanks or catamaran ships.

For floating bodies of general shape, it has been customary to separate wave and current

effects, computing the wave forces at zero forward speed. However, this is not satisfactory because the forward speed may alter the wave forces considerably. More recently, Chang (1977) and Inglis and Price (1981) have taken account of the coupling between waves and current partially by including the constant forward speed in the boundary conditions, but neglecting the steady disturbance imposed by the body. This gives an inconsistently linearized three-dimensional theory. The agreement with experiment is only partially satisfying. In particular, the roll and pitch damping are very unsatisfactory. This indicates that the steady disturbance of the body may be important.

In many practical problems, the actual forward speed may be quite small, especially in the case of oil platforms. Perturbation expansions can then be used with respect to both wave amplitude and forward speed. If the problem is solved to first order in the forward speed, a rigid wall condition applies on the free surface in the steady problem. This approach has been used by Zhao and Faltinsen (1987,1989), who found that even a small forward speed affects the wave drift force significantly. They used a hybrid method, with the velocity potential being represented by a boundary integral in the inner domain and by a multipole expansion in the outer domain.

We will examine the problem somewhat differently, using a boundary element method where the solution is expressed as an integral over the wetted body surface and the free surface. By using a Green function satisfying the correct radiation condition, we will not need to discretize any control surface far away from the body, as is necessary with methods using a Rankine singularity as the Green function. Also, the contribution from the free surface decays rapidly with increasing distance from the body, and is thus easy to handle numerically.

To solve the integral equations, the velocity potential is expanded in an asymptotic series in powers of the dimensionless forward speed (reduced frequency), retaining linear terms. This expansion is not uniformly valid, and is therefore only used in the vicinity of the body. (When we calculate the potential far away from the body, we return to the unperturbed integral equations.) Perturbing the equations moves the free surface integral, which is of higher order in the reduced frequency, to the right hand side of the integral equations, thus reducing the number of unknowns necessary for numerical solution. We will also show that applying the correct boundary condition on the body in the steady problem eliminates the usual waterline integral for wall-sided bodies, as opposed to the methods of Chang or Inglis and Price, where the neglection of the steady disturbance potential in the free surface condition leads to integral equations containing a waterline integral.

A special numerical problem arises if the body has sharp edges. The boundary condition is ill-posed at sharp edges and corners, and the resulting boundary integrals are

not integrable. This is circumvented by rewriting the integral equations using a special variety of Stokes' theorem known to marine hydrodynamicists as Tuck's theorem (Ogilvie and Tuck, 1969). This reduces the order of the derivatives in the body boundary condition by one, rendering the boundary integrals singular but integrable.

In the integral formulation, we need to calculate the translating pulsating source in three dimensions. This function is in general hard to compute efficiently. However, since the forward speed is small, we can use an asymptotic expansion of the source potential which only involves the zero-speed pulsating source and its derivatives.

When the potential has been found, the first order forces can be found by simple pressure integration over the body. The Timman-Newman symmetry relations for the added mass and damping are derived for the case when the steady double-body flow around the body is included in the free surface condition, which has not been done in previous theories (Timman and Newman (1962), Newman(1978)). A far-field form of the Haskind relations with forward speed is derived. The mean second-order force is obtained by far-field analysis, and the energy equation for the diffraction problem is derived. This is used to check the consistency of the results. All the derivations are made for an arbitrary heading angle of the incident wave.

In summary, the advantages of the present method are:

- The wave motion is described by simple integral equations that are well suited for evaluating wave forces.
- We consistently include all first-order forward-speed effects, and simultaneously simplify the equations by linearizing the equations in the forward speed.
- The Green function takes proper care of the radiation condition, even with a variable-coefficient free surface condition.
- The fast-decaying free surface integral is easy to compute numerically.
- Corner singularities are treated more easily by means of Tuck's thorem.
- Linearization with respect to forward speed simplifies the computation of the Green function.
- The Timman-Newman relations are satisfied even with the variable-coefficient free surface condition.
- Both the linear exciting force and the wave drift force with forward speed are expressed by simple far-field quantities for an arbitrary wave heading.

Numerical examples are presented for several different body geometries and ranges of parameters, and with extensive convergence tests. It is found that for a body of simple shape, the wave drift damping is usually positive, while for a body of more complicated shape, interference between different parts of the structure may lead to negative wave drift damping for some frequencies. Some of the results are compared to the results of Zhao and Faltinsen (1989), with quite good agreement.

Chapter 2

The integral equations

In this chapter, we will develop the governing equations for the fluid motion. No restrictions are made upon the shape of the body, except that lifting or cavitating surfaces are not allowed. We will assume that the incident waves are long-crested and regular. Viscous effects are also neglected, assuming that the body is large compared to the wave amplitude. In the common jargon of marine hydrodynamics, this means that the Keulegan-Carpenter number is small. It is also assumed that boundary layer separation due to the steady flow has negligible effect on the wave forces. With these assumptions, linear potential theory may be applied. We can then use Green's second identity to obtain a set of boundary integral expressions for the radiation and diffraction potentials and the steady potential.

2.1 The boundary value problem

In this section we will state the boundary value problem for the velocity potential. We consider a body B moving horizontally with constant forward speed U and responding to long-crested regular incoming waves with small amplitude A. We will use a reference frame (x, y, z) moving in the same direction as the body with forward speed U, with the undisturbed free surface in the xy-plane, the x-axis in the direction of forward motion, and the z-axis vertically upwards. In this reference frame the body is performing small oscillations due to the incoming waves, while situated in a uniform current $-U$ at infinity. This configuration is shown in Fig. 2.1. We assume the fluid to be homogeneous, incompressible, and of infinite extent in the lower half-space. Viscosity and surface tension are neglected. Then there exists a velocity potential ϕ for the velocity $\mathbf{v} = \nabla\phi$ that satisfies Laplace's equation

$$\nabla^2\phi = 0 \tag{2.1}$$

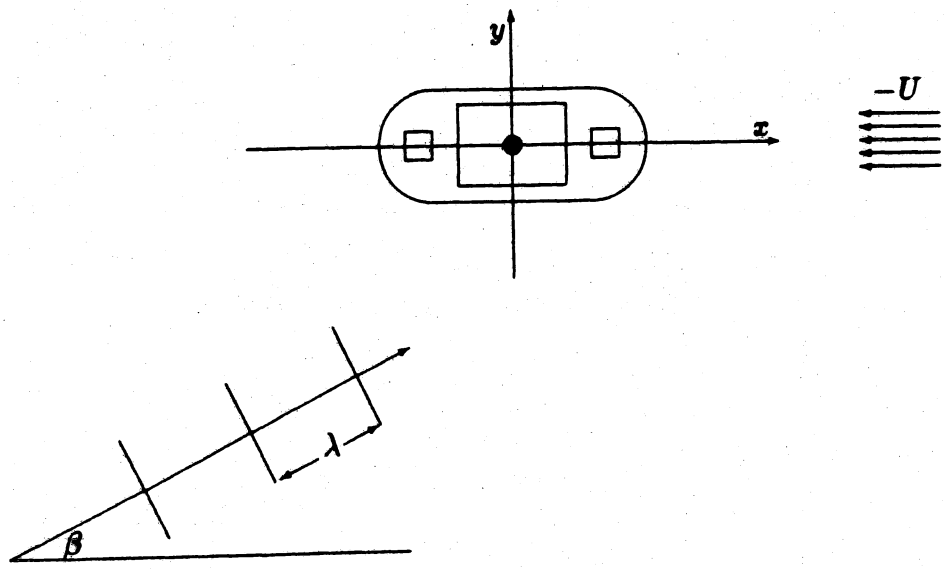

Figure 2.1: Coordinate system with incoming waves and current.

To first order in the wave amplitude, the velocity potential may be written

$$\phi = \phi_s(\boldsymbol{x}) + \phi_D(\boldsymbol{x}, t) + \phi_R(\boldsymbol{x}, t) \tag{2.2}$$

where ϕ_s is independent of time, and ϕ_D and ϕ_R are time harmonic with orbital frequency σ. The steady potential ϕ_s may be written

$$\phi_s = U(\chi - x) \tag{2.3}$$

where $-Ux$ is the ambient uniform current and $U\chi$ is the steady disturbance due to the body. ϕ_R is the total radiation potential due to the motions of the body, which may be written

$$\phi_R = \text{Re } i\sigma e^{i\sigma t} \sum_{j=1}^{6} \xi_j \phi_j(\boldsymbol{x}) \tag{2.4}$$

where ξ_j is the amplitude of motion in the jth mode (surge, sway, heave, roll, pitch and yaw respectively), and ϕ_j is the corresponding radiation potential for unit amplitude of motion. ϕ_D is the total diffraction potential, and may be written

$$\phi_D = \text{Re } A e^{i\sigma t}(\phi_0(\boldsymbol{x}) + \phi_7(\boldsymbol{x})) \tag{2.5}$$

where ϕ_7 is the scattering potential, and ϕ_0 is the potential due to the incoming waves :

$$\phi_0 = \frac{ig}{\omega} e^{Kz} e^{-iK(x\cos\beta + y\sin\beta)} \tag{2.6}$$

Here $K = \omega^2/g$ is the zero speed wavenumber, and ω is the orbital frequency of the incoming wave, given by

$$\omega = \sigma + UK\cos\beta \tag{2.7}$$

β is the incidence angle of the incoming waves. The case $\beta = 0$ corresponds to following waves, while $\beta = \pi$ corresponds to head waves. The frequency σ is called the frequency of encounter.

2.1.1 The boundary conditions on the body

The steady potential fullfills the body boundary condition

$$\frac{\partial \chi}{\partial n} = n_1 \text{ on } S_B \tag{2.8}$$

corresponding to zero flux through the wetted surface. (n_1, n_2, n_3) denotes the Cartesian components of the normal vector $\mathbf{n}$ pointing out of the fluid domain. The body boundary condition for the unknown potentials ϕ_j, $j = 1, \ldots, 7$, are (Newman, 1978)

$$\frac{\partial \phi_j}{\partial n} = \begin{cases} n_j + \frac{U}{i\sigma} m_j, & j = 1, \ldots, 6 \\ -\frac{\partial \phi_S}{\partial n}, & j = 7 \end{cases} \tag{2.9}$$

where $(n_4, n_5, n_6) = \boldsymbol{x} \times \mathbf{n}$. m_j, $j = 1, 2, 3$ are the components of the vector

$$\mathbf{m} = -\mathbf{n} \cdot \nabla(\nabla \chi_s) \tag{2.10}$$

and m_j, $j = 4, 5, 6$ are the components of the vector

$$\mathbf{m}' = -\mathbf{n} \cdot \nabla(\boldsymbol{x} \times \nabla \chi_s) \tag{2.11}$$

where

$$\chi_s = \chi - x \tag{2.12}$$

Thus, the normal derivative of each radiation potential has two parts. The first, the n-term, represents the normal velocity at the mean position of the body, while the second, the m-term, represents the change in the local steady field due to the motion of the body. Computing the m-terms accurately usually represents a difficult numerical problem. In our case, this is circumvented by replacing the m-terms in the boundary integral formulation by first-order derivatives of χ, using a variant of Stokes' thorem known as Tuck's thorem (Ogilvie and Tuck,1969). This is described in Section 2.5.

2.1.2 The boundary conditions on the free surface

Let ℓ be a characteristic dimension of B. If the Froude number $Fr = U/\sqrt{g\ell}$ is much less than one, the free surface condition for the steady potential can be approximated by

$$\frac{\partial \phi_s}{\partial z} = 0 \text{ at } z = 0 \tag{2.13}$$

to first order in the Froude number. The radiation potentials ϕ_j and the diffraction potential ϕ will then satisfy the free surface condition

$$-\sigma^2\phi + 2i\sigma\nabla_1\phi_s \cdot \nabla_1\phi + i\sigma\phi\nabla_1^2\phi_s + g\frac{\partial\phi}{\partial z} = 0 \text{ at } z = 0 \tag{2.14}$$

to the same order. When ϕ_s is precalculated, this is a linear boundary condition with variable coefficients. ∇_1 here means the horizontal gradient. Far away from the body, $\phi_s = -Ux$, and (2.14) simplifies to the linear boundary condition

$$-\sigma^2\phi - 2i\sigma U\frac{\partial\phi}{\partial x} + g\frac{\partial\phi}{\partial z} = 0 \text{ at } z = 0 \tag{2.15}$$

which only contains known constant coefficients.

2.2 The steady problem

The steady problem for small Froude numbers, with the rigid wall condition (2.13) on the free surface, can easily be solved with a boundary integral method. We define a Green function

$$g(\boldsymbol{x}, \boldsymbol{\xi}) = \frac{1}{r} + \frac{1}{r'} \tag{2.16}$$

where

$$r = \sqrt{(x-\xi)^2 + (y-\eta)^2 + (z-\zeta)^2} \tag{2.17}$$

and

$$r' = \sqrt{(x-\xi)^2 + (y-\eta)^2 + (z+\zeta)^2} \tag{2.18}$$

$g(\boldsymbol{x}, \boldsymbol{\xi})$ is the potential of a source of strength -4π placed in the point $\boldsymbol{\xi} = (\xi, \eta, \zeta)$ which satisfies the rigid wall free surface condition (2.13). We now represent the potential in the fluid as a distribution of sources of strength $Q(x, y, z)$ over the body:

$$\chi(\boldsymbol{x}) = \frac{1}{4\pi}\iint_{S_B} Q(\boldsymbol{\xi})g(\boldsymbol{x}, \boldsymbol{\xi})dS \tag{2.19}$$

Applying the boundary condition (2.8) at a field point $\boldsymbol{x}$ on the body surface, we get

$$2\pi Q(\boldsymbol{x}) + \iint_{S_B} Q(\boldsymbol{\xi})\frac{\partial g(\boldsymbol{x}, \boldsymbol{\xi})}{\partial n_{\boldsymbol{x}}}dS = 4\pi n_1 \tag{2.20}$$

This integral equation can easily be solved by a collocation method.

2.3 The oscillatory problems

We will now consider solving the radiation and diffraction problems with the boundary condition (2.14) at the free surface and the boundary condition (2.9) on the wetted body surface. We will solve the boundary value problems by applying Green's second identity to the entire fluid domain. As the Green function we will use a pulsating source translating with small forward speed and satisfying the free surface condition

$$-\sigma^2 G + 2i\sigma U\frac{\partial G}{\partial \xi} + g\frac{\partial G}{\partial \zeta} = 0 \text{ at } \zeta = 0 \tag{2.21}$$

plus an appropriate radiation condition. Following Huijsmanns and Hermans (1985), the Green function can be expanded in an asymptotic series in powers of the parameter

$$\tau = \frac{U\sigma}{g} \tag{2.22}$$

which is often called the reduced frequency. The first two terms in this series can be computed from the zero forward speed pulsating source and its first-order spatial derivatives. This is shown in Section 3.2. The series expansion is not uniformly valid, but is asymptotically valid as $\tau \to 0$ at any finite distance from the origin.

First we will develop the equation for the diffraction potential. The variable-coefficient condition (2.14) must be used for ϕ on the free surface, while the constant-coefficient condition (2.21) is used for the forward-speed Green function. Let S_F denote the undisturbed free surface $z = 0$, and let S_∞ denote a vertical cylinder enclosing the fluid at infinity. We apply Green's theorem to $\phi = \phi_0 + \phi_7$ and G, and introduce the boundary condition (2.9) on the body. This yields

$$\iint_{S_B} \phi\frac{\partial G}{\partial n}dS + \iint_{S_F}\left(\phi\frac{\partial G}{\partial n} - G\frac{\partial \phi}{\partial n}\right)dS + \iint_{S_\infty}\left(\phi\frac{\partial G}{\partial n} - G\frac{\partial \phi}{\partial n}\right)dS = \begin{cases} -4\pi\phi(\boldsymbol{x}) \\ -2\pi\phi(\boldsymbol{x}) \end{cases} \tag{2.23}$$

where the first case applies to $\boldsymbol{x}$ in the fluid domain and the second to $\boldsymbol{x}$ on the wetted body surface.

Let C_B denote the waterline curve of the body, and C_∞ the waterline curve of S_∞. For the integral over the free surface in (2.23), (2.14) and the two-dimensional divergence theorem applied on the free surface gives

$$\begin{aligned}\iint_{S_F}\left(\phi\frac{\partial G}{\partial n} - G\frac{\partial \phi}{\partial n}\right)dS = &- 2i\tau\iint_{S_F}\phi(\nabla_1 G\cdot\nabla_1\chi + \frac{1}{2}G\nabla_1^2\chi)dS \\ &- 2i\tau\int_{C_\infty}\phi G d\eta + 2i\tau\int_{C_B}\phi G\left(\frac{\partial \chi}{\partial n} - n_1\right)ds\end{aligned} \tag{2.24}$$

We have assumed that the body is wall-sided at the free surface to obtain the waterline integral on the form above. Applying the boundary condition (2.8) for χ, we see that the body waterline integral in (2.24) vanishes exactly. This would not have been the case if we had neglected the steady disturbance χ in the free surface condition (2.14), as has been done by for instance Chang (1977) and Inglis and Price (1981).

We now want to eliminate the integral over S_∞ in (2.23) and the integral over C_∞ in (2.24). By using the far-field behaviour of the scattering potential, which is given in (5.1), we can easily show that

$$\iint_{S_\infty} \left(\phi_7 \frac{\partial G}{\partial n} - G \frac{\partial \phi_7}{\partial n} \right) dS - 2i\tau \int_{C_\infty} \phi_7 G d\eta = 0 \tag{2.25}$$

(For details, see Appendix A).. Thus, the contributions from ϕ_7 to the integrals over the far-field in (2.23) and (2.24) cancel each other.

To eliminate the contributions from ϕ_0 to the far-field integrals in (2.23) and (2.24), we apply Green's theorem to ϕ_0 and G in the entire lower half-space, with the result

$$\iint_{S_\infty} \left(\phi_0 \frac{\partial G}{\partial n} - G \frac{\partial \phi_0}{\partial n} \right) dS - 2i\tau \int_{C_\infty} \phi_0 G d\eta = -4\pi\phi_0 \tag{2.26}$$

where C_∞ is a closed curve enclosing the free surface at infinity. Eliminating the integrals over S_∞ and C_∞ from the integral equation by using (2.25) and (2.26), we get the Fredholm equation

$$\iint_{S_B} \phi \frac{\partial G}{\partial n} dS - 2i\tau \iint_{S_F} \phi (\nabla_1 G \cdot \nabla_1 \chi + \frac{1}{2} G \nabla_1^2 \chi) dS - 4\pi\phi_0 = \begin{cases} -4\pi\phi(\boldsymbol{x}) \\ -2\pi\phi(\boldsymbol{x}) \end{cases} \tag{2.27}$$

where the first case applies to $\boldsymbol{x}$ in the fluid domain and the second to $\boldsymbol{x}$ on the wetted body surface.

Using the boundary condition (2.9) on the body, the corresponding result for the radiation problems can be shown to be

$$\iint_{S_B} \left(\phi_j \frac{\partial G}{\partial n} - G(n_j + \frac{U}{i\sigma} m_j) \right) dS - 2i\tau \iint_{S_F} \phi_j (\nabla_1 G \cdot \nabla_1 \chi + \frac{1}{2} G \nabla_1^2 \chi) dS = \begin{cases} -4\pi\phi_j(\boldsymbol{x}) \\ -2\pi\phi_j(\boldsymbol{x}) \end{cases} \tag{2.28}$$

for $j = 1, \ldots, 6$.

The integral equations (2.27) – (2.28) display some important differences from those usually seen in ship hydrodynamics. In the full linear three-dimensional problem, the steady disturbance χ is usually neglected. Applying Greens's theorem then leads to integral equations containing a waterline integral, as in the papers of Chang (1977) and Inglis and Price (1981). In our case, this integral vanishes because the steady potential $U(\chi - x)$

is satisfying the correct boundary condition (2.8) on the body surface. Instead of the waterline integral, our equations contain an integral over the free surface. This integral, however, decays very rapidly with increasing distance from the body, since it contains the spatial derivatives of the steady disturbance χ, and χ behaves as a dipole far from the body. Therefore we may always truncate the free surface at a quite short distance from the body.

2.4 Perturbation procedure

We now want to solve the integral equations (2.27) and (2.28) for the unknown potentials ϕ_j and ϕ_D on the body. To simplify the equations further, we assume that the reduced frequency $\tau \ll 1$, and expand ϕ and G in asymptotic series of τ, keeping only linear terms:

$$\phi = \phi^0 + \tau\phi^1 \tag{2.29}$$

$$G = G^0 + \tau G^1 \tag{2.30}$$

It must be emphasized that these expansions are local, and only valid at finite distance from the origin.

Introducing the asymptotic expansions into (2.27) and (2.28) and collecting terms of the same order in τ, we find the two sets of integral equations

$$2\pi\phi_j^0 + \iint_{S_B} \phi_j^0 \frac{\partial G^0}{\partial n} dS = \begin{cases} \iint_{S_B} G^0 n_j dS, & j = 1, \ldots, 6 \\ 4\pi\phi_0, & j = D \end{cases} \tag{2.31}$$

$$\begin{aligned} 2\pi\phi_j^1 + \iint_{S_B} \phi_j^1 \frac{\partial G^0}{\partial n} dS &= 2i \iint_{S_F} \phi_j^0 (\nabla_1 G^0 \cdot \nabla_1 \chi + \frac{1}{2} G^0 \nabla_1^2 \chi) dS \\ - \iint_{S_B} \phi_j^0 \frac{\partial G^1}{\partial n} dS &+ \begin{cases} \iint_{S_B} \left(G^1 n_j + G^0 \frac{m_j}{i\omega} \right) dS, & j = 1, \ldots, 6 \\ 0, & j = D \end{cases} \end{aligned} \tag{2.32}$$

where $j = D$ means the diffraction problem. The zero in the right hand side of the diffraction problem stems from the fact that the incident-wave potential ϕ_0 is independent of τ.

The series expansion simplifies the problem considerably. Since the free surface integral is higher order than the other terms, it will only occur at the right-hand side. Thus, when discretizing the equations, we only need to solve for the unknown potentials ϕ^0 and ϕ^1 on the body, not at the free surface.

In addition, the free surface integral decays very rapidly. Since the steady disturbance χ behaves like a dipole, the integrand decays like R^{-4}, where R is the polar radius. Thus, it is only necessary to discretize the free surface out to 2-3 body diameters.

2.5 The right hand sides in the radiation problems

The right-hand sides in the integral equations for the radiation potentials contain the m-terms, which are given by (2.10) – (2.11). These terms are awkward to compute numerically, since they are normal derivatives of the steady velocity. The steady velocity itself can easily be obtained by differentiating (2.19) analytically, but the corresponding second derivatives leads to non-existent integrals, so apparently the m-terms must be obtained by the undesirable method of numerical differentiation. However, the right-hand sides can be rewritten using Tuck's theorem (Ogilvie and Tuck, 1969), which states that for any differentiable function f, is

$$\iint_{S_B} \nabla\chi_s \cdot \nabla f n_i dS = -\iint_{S_B} f m_i dS - \int_{C_B} f \frac{\partial \chi}{\partial z} n_i ds \tag{2.33}$$

provided that the wetted surface S_B is smooth and that it is wall-sided at the free surface. In our case, the waterline contribution in Tuck's theorem vanishes due to the rigid wall condition (2.13).

However, the function corresponding to f in the right hand side in (2.32) is $G^0(\boldsymbol{x}, \boldsymbol{\xi})$, which is not differentiable at $\boldsymbol{x} = \boldsymbol{\xi}$.However, if we put $\boldsymbol{x}$ in the fluid and let it approach the body, we find that both sides of (2.33) are continuous as $\boldsymbol{x} \to S_B$. This is explained in Appendix B. Thus, the integral equations (2.32) can be rewritten as

$$\begin{aligned} 2\pi\phi_j^1 + \iint_{S_B} \phi_j^1 \frac{\partial G^0}{\partial n} dS = 2i \iint_{S_F} \phi_j^0 (\nabla_1 G^0 \cdot \nabla_1 \chi + \frac{1}{2} G^0 \nabla_1^2 \chi) dS \\ - \iint_{S_B} \phi_j^0 \frac{\partial G^1}{\partial n} dS + \iint_{S_B} \left(G^1 - \frac{1}{i\nu} \nabla G^0 \cdot \nabla \chi_s \right) n_j dS, j = 1, \ldots, 6 \end{aligned} \tag{2.34}$$

which only contains first-order derivatives of the steady potential.

For a body with sharp edges, Tuck's theorem is not valid. In fact, even the boundary condition (2.9) is invalid in this case. (2.9) originates from a Taylor expansion of the time-domain boundary condition. This expansion is only valid for smooth surfaces. The result is that the m-terms not even are integrable at an edge. Still, frequency-domain analysis with the boundary condition (2.9) is often used, since most offshore structures have sharp edges and corners.

With our reformulation, however, the right hand side is integrable as long as the field point is not situated directly at the edge. Therefore we believe that this formulation will lead to a better numerical behaviour at the edge.

Chapter 3

Numerical methods

3.1 Solution of the integral equations

The integral equations (2.20), (2.31) and (2.32) are solved by a conventional panel method. The body is approximated by plane quadrilateral elements, and the velocity potential is assumed constant over each panel. The quadrilaterals may degenerate to triangles. Using the panel centroids as collocation points, the integral equations are reduced to sets of complex linear equations which for a moderate number of panels may be solved by Gaussian elimination.

To compute the free surface integral, the free surface is panelized in the same manner as the wetted body surface. However, since this term only contributes to the right hand sides of the equations, this means very little additional computer memory usage. The free surface is truncated at about 3 body diameters' distance from the center of the body.

In all the calculations, the singular terms of the various Green functions are integrated by the Hess and Smith method. The logarithmic singularities have been integrated by the method of Newman and Sclavounos (1987). Numerical integrations over each panel are performed using mainly the mid-point rule. Our program is also designed to use four-point Gaussian quadrature over each panel. Experience shows that this does not improve the results significantly, and the four-point method increases the total CPU time of the computations by a factor of about 2 compared to the mid-point method.

No special algorithms are used to take care of the corner singularitites for bodies with sharp corners. However, since the integral formulation (2.34) is used, the right hand sides in the radiation problems are integrable. The errors associated with these terms are therefore assumed to be small.

3.2 The Green function

The translating pulsating source with small forward speed has been discussed by Huijsmans and Hermans (1985), and we will use a similar procedure. We assume that the parameter $\tau = U\sigma/g < 1/4$. The translating pulsating source can be written as (see, for example, Newman, 1959)

$$G(\boldsymbol{x},\boldsymbol{\xi}) = \frac{1}{r} - \frac{1}{r'} + \Psi(\boldsymbol{x},\boldsymbol{\xi}) \tag{3.1}$$

with r and r' given by (2.17) and (2.18) and

$$\Psi(\boldsymbol{x},\boldsymbol{\xi}) = \frac{1}{\pi}\int_0^{2\pi}\int_{L_1} \frac{E(\theta,k)dkd\theta}{(k-\kappa_1)\sqrt{1+4\tau\cos\theta}}$$
$$-\frac{1}{\pi}\int_{-\pi/2}^{\pi/2}\int_{L_2} \frac{E(\theta,k)dkd\theta}{(k-\kappa_2)\sqrt{1+4\tau\cos\theta}} - \frac{1}{\pi}\int_{\pi/2}^{3\pi/2}\int_{L_2'} \frac{E(\theta,k)dkd\theta}{(k-\kappa_2)\sqrt{1+4\tau\cos\theta}} \tag{3.2}$$

where

$$E(\theta,k) = k\exp\left[k(z+\zeta) + ik\left((x-\xi)\cos\theta + (y-\eta)\sin\theta\right)\right] \tag{3.3}$$

where the poles κ_1 and κ_2 are given by

$$\kappa_{1,2} = \frac{\nu}{2\tau^2\cos^2\theta}\left[1+2\tau\cos\theta \mp \sqrt{1+4\tau\cos\theta}\right] \tag{3.4}$$

and the integration path L_1 passes above the pole at κ_1 while the paths L_2 and L_2' pass below and above the pole at κ_2, respectively, and

$$\nu = \frac{\sigma^2}{g} \tag{3.5}$$

It is easily seen that as $\tau \to 0$, $\kappa_1 \to \nu$ and $\kappa_2 \to \infty$. Thus, κ_1 approaches the zero-speed wavenumber, while the κ_2 waves get infinitely short. We will use a Green function without the κ_2 terms, which corresponds to neglecting U^2 in the free surface condition.

We now expand the first term in Ψ, which we call ψ, in powers of τ :

$$\psi = \psi_0 + \tau\psi_1 + \ldots \tag{3.6}$$

This is an asymptotic expansion, which is not uniformly valid. It can be used locally, but not at infinite distance from the source point. ψ_0 is the zero-speed source potential given by

$$\psi_0 = 2\int_0^\infty \frac{ke^{k(z+\zeta)}}{k-\nu} J_0(kR)dk \tag{3.7}$$

where $R = \sqrt{(x-\xi)^2+(y-\eta)^2}$, J_0 is the Bessel function of the first kind and zero order, and the integration passes above the pole. To first order in τ, we have that

$$\kappa_1 = \nu(1-2\tau\cos\theta) \tag{3.8}$$

and thus

$$\frac{1}{(k-\kappa_1)\sqrt{1+4\tau\cos\theta}} = \frac{k-\nu-2\tau k\cos\theta}{(k-\nu)^2} + \mathcal{O}(\tau^2) \tag{3.9}$$

Using this expression to expand ψ, we find that

$$\psi_1 = -4i\frac{x-\xi}{R}\int_0^\infty \frac{k^2 e^{k(z+\zeta)}}{(k-\nu)^2} J_1(kR)dk \tag{3.10}$$

where J_1 is the Bessel function of the first kind and first order, and the integration passes above the pole. We note that

$$\psi_1 = 2i\frac{\partial^2\psi_0}{\partial\nu\partial x} \tag{3.11}$$

a remarkable result which will be used later. The zero-speed Green function involves the integral ψ_0 given by (3.7), which may also be written as

$$\psi_0 = 2\left(\frac{1}{r'} + \nu I - \pi i\nu e^{\nu(z+\zeta)}J_0(\nu R)\right) \tag{3.12}$$

where the integral I is given by

$$I = \mathrm{PV}\int_0^\infty \frac{e^{k(z+\zeta)}}{k-\nu} J_0(kR)dk \tag{3.13}$$

where PV denotes the Cauchy principal value. Inserting the last expression for ψ_0 into (3.11), we get

$$\psi_1 = -4\pi\frac{x-\xi}{R}\frac{d}{d\nu}\left(\nu^2 e^{\nu(z+\zeta)}J_1(\nu R)\right) + 4i\frac{x-\xi}{R}[1+\nu(z+\zeta)]\frac{\partial I}{\partial R} - 4i\nu(x-\xi)\left(\frac{1}{r'}+\nu I\right) \tag{3.14}$$

Thus, the Green function for small forward speed, given by (3.6), (3.12) and (3.14) can be expressed by means of the real and imaginary parts of the zero-speed Green function and its first order derivatives. The numerical integration of (3.14) and its normal derivative over each panel of the body surface is described in Appendix C.

3.3 The far-field expansion of the Green function

When we compute the mean second-order wave forces on the body, we will use far-field analysis, in which we need to know the velocity potential as $R \to \infty$. From the integral formulations (2.27) and (2.27), we see that we then need to compute the Green function with forward speed at large distances from the origin.

Newman (1959) has developed the far-field expansion of the Green function with arbitrary forward speed for $R \to \infty$. Haskind (1946) has given a far-field expansion of the

Green function for small values of τ. Since there seems to be a disagreement between the expressions of Newman and Haskind, we have found it necessary to recompute the far-field expansion for small τ. Let us introduce cylindrical coordinates $x = R\cos\theta$, $y = R\sin\theta$. Using contour integration and the method of stationary phase, we find that for large R,

$$G(R,\theta,z;\xi,\eta,\zeta) = k_1(\theta_0)\sqrt{\frac{8\pi}{\nu R}}e^{k_1(\theta_0)[z+\zeta-iR+i\xi\cos\theta_0+i\eta\sin\theta_0]-i\pi/4}(1+\mathcal{O}(\tau^2,R^{-1/2})) \quad (3.15)$$

where the wave number is

$$k_1(\theta_0) = \frac{\nu}{2\tau^2\cos^2\theta_0}\left[1-2\tau\cos\theta_0-\sqrt{1-4\tau\cos\theta_0}\right] \quad (3.16)$$

where the relation between the wave angle θ_0 and the space angle θ is given in Newman (1959) for arbitrary values of τ. (3.15) agrees with Newman (1959) to first order in τ.

We are only interested in using the far-field expansion (3.15) of the Green function to compute wave forces at small forward speed. In this context, the wave number k_1 may be written

$$k_1(\theta_0) = \nu(1+2\tau\cos\theta_0)+\mathcal{O}(\tau^2) \quad (3.17)$$

where the relation between the wave angle θ_0 and the spatial angle θ is given by

$$\theta_0 = \theta - 2\tau\sin\theta + \mathcal{O}(\tau^2) \quad (3.18)$$

corresponding to an outgoing ring wave pattern with waves that are slightly shorter upstream than downstream.

Introducing this value of the wave number into (3.15) and expanding, we find that the final expression for the Green function may be written

$$G(R,\theta,z;\xi,\eta,\zeta) = R^{-1/2}h(\xi,\theta)e^{k_1(\theta)(z-iR)}+\mathcal{O}\left(\frac{1}{R}\right) \quad (3.19)$$

where the amplitude $h(\xi,theta)$ is given by

$$h(\xi,\theta) = \sqrt{\frac{8\pi}{\nu}}k_1(\theta)e^{k_1(\theta)[\zeta+i\xi(\cos\theta+2\tau\sin^2\theta)+i\eta(\sin\theta-2\tau\cos\theta\sin\theta)]-i\pi/4}+\mathcal{O}(\tau^2) \quad (3.20)$$

The far-field expansion of the Green function on the form (3.19) will be used in the two next chapters to derive simple expressions for the linear exciting forces, the mean second-order drift force and the energy flux at infinity in the diffraction problem, by applying the method of stationary phase.

Chapter 4

The first-order wave forces

Having found the velocity potential by the method presented in the previous sections, the first-order wave forces can now be found by pressure integration over the body surface. We will now develop some useful formulae for the forces and examine some important properties of the added mass and damping coefficients and the linear exciting force coefficients.

4.1 Added mass and damping

The added mass and damping coefficients can now be obtained from the radiation potentials. Denoting the added mass coefficients by a_{ij} and the damping coefficients by b_{ij}, we can express the radiation force and moment as

$$F_i = \mathrm{Re}\left(-i\sigma\xi_j e^{i\sigma t} f_{ij}\right) \tag{4.1}$$

where $i, j = 1, \ldots, 6$, and the complex force coefficients f_{ij} are defined as

$$f_{ij} \equiv i\sigma a_{ij} + b_{ij} = \rho \iint_{S_B} (i\sigma\phi_j + \nabla\phi_s \cdot \nabla\phi_j) n_i dS \tag{4.2}$$

We now use Tuck's theorem (2.33), obtaining

$$f_{ij} = \rho \iint_{S_B} (i\sigma n_i - U m_i)\phi_j dS \tag{4.3}$$

Timman and Newman (1962) have shown that when the steady disturbance field χ is neglected in the free surface condition (2.14), the added mass and damping satisfy the so-called Timman-Newman relations

$$f_{ij}(U) = f_{ji}(-U), \qquad i, j = 1, \ldots, 6 \tag{4.4}$$

That is, the hydrodynamic forces are the same when we reverse the forward speed and exchange indices.

Newman (1978) has also shown that the added mass and damping coefficients satisfy these relations in the special case of a slender ship, with the steady disturbance χ neglected in the free surface condition. We will now use the formula (4.3) to show that these relations are also satisfied with the free surface condition (2.14) including χ used instead of the usual free surface condition without χ, and for a body of arbitrary shape. To show this, we introduce the reversed-flow radiation potentials ψ_j, which satisfiy the boundary conditions (2.9) and (2.14) with the sign of U reversed. Thus, we have

$$\frac{\partial \psi_j}{\partial n} = n_j - \frac{U}{i\sigma} m_j, j = 1, \ldots, 6 \tag{4.5}$$

$$-\sigma^2 \psi_j - 2i\sigma U \nabla_1 \chi \cdot \nabla_1 \psi_j + 2i\sigma U \frac{\partial \psi_j}{\partial x} - i\sigma U \psi_j \nabla_1^2 \chi + g \frac{\partial \psi_j}{\partial z} = 0 \text{ at } z = 0 \tag{4.6}$$

Using the definition of ψ_j, we can write

$$f_{ij}(U) = i\sigma\rho \iint_{S_B} \phi_j \frac{\partial \psi_i}{\partial n} dS \tag{4.7}$$

$$f_{ji}(-U) = i\sigma\rho \iint_{S_B} \psi_i \frac{\partial \phi_j}{\partial n} dS \tag{4.8}$$

Applying Green's theorem to ϕ_j and ψ_i, we obtain

$$f_{ij}(U) - f_{ji}(-U) = i\sigma\rho \iint_{S_B} \left(\phi_j \frac{\partial \psi_i}{\partial n} - \psi_i \frac{\partial \phi_j}{\partial n} \right) dS =$$

$$-i\sigma\rho \iint_{S_F} \left(\phi_j \frac{\partial \psi_i}{\partial n} - \psi_i \frac{\partial \phi_j}{\partial n} \right) dS - i\sigma\rho \iint_{S_\infty} \left(\phi_j \frac{\partial \psi_i}{\partial n} - \psi_i \frac{\partial \phi_j}{\partial n} \right) dS \tag{4.9}$$

Using the free surface conditions (2.14) and (4.6) and the two-dimensional divergence theorem, the integral over the free surface can be written

$$-\iint_{S_F} \left(\phi_j \frac{\partial \psi_i}{\partial n} - \psi_i \frac{\partial \phi_j}{\partial n} \right) dS = -2i\tau \iint_{S_F} \nabla_1 \cdot (\phi_j \psi_i \nabla_1 \chi_s) dS \tag{4.10}$$

$$= 2i\tau \int_{C_B} \phi_j \psi_i \frac{\partial \chi_s}{\partial n} ds + 2i\tau \int_{C_\infty} \phi_j \psi_i dy \tag{4.11}$$

We have assumed that the body is wall-sided at the free surface. Using the body boundary condition (2.8) for $\chi_s = \chi - x$, we find that the waterline integral vanishes. To evaluate the other integrals, we need the far-field behaviour of the radiation potentials ϕ_i and ψ_j. To obtain this behaviour, we consider the Green function. The far-field expression for the Green function is given by (3.19). From the integral equations (2.28), we see that the

radiation potentials must have the same behaviour with respect to the field point as the Green function when $R \to \infty$. From (3.19) we see that this behaviour must be

$$\phi_j = R^{-1/2} H_j(\theta;\tau) e^{\nu(1+2\tau\cos\theta)(z-iR)(1+\mathcal{O}(\tau^2))}(1+\mathcal{O}(\tau^2, R^{-1/2})) \tag{4.12}$$

as $R \to \infty$, where $H_j(\theta)$ is the far-field amplitude distribution of the jth radiation potential.

The amplitude distributions $H_j(\theta)$ are obtained by inserting the far-field expansion (3.19) of the Green function into the integral equations (2.28). We then use Tuck's theorem (2.33) to replace the m-terms by the steady velocity $\nabla\chi_s$ in the amplitude distributions of the radiation potentials. This yields the following expressions for the amplitude distributions:

$$H_j(\theta) = \iint_{S_B} \left(\phi_j \frac{\partial h}{\partial n} - (h - \frac{\tau}{i\nu}\nabla\chi_s \cdot \nabla h)n_j\right) dS - 2i\tau \iint_{S_F} \phi_j(\nabla_1 h \cdot \nabla_1 \chi + \frac{1}{2} h \nabla_1^2 \chi) dS \tag{4.13}$$

for $j = 1, \ldots, 6$, where the amplitude $h(\xi, \theta)$ of the Green function is given by (3.20).

The expression for ψ_i corresponding to (4.12) is obtained by reversing the sign of τ, that is,

$$\psi_j = R^{-1/2} H_j(\theta;-\tau) e^{\nu(1-2\tau\cos\theta)(z-iR)(1+\mathcal{O}(\tau^2))}(1+\mathcal{O}(\tau^2, R^{-1/2})) \tag{4.14}$$

Inserting these expressions into the integral over S_∞ and integrating with respect to z, we find that this integral exactly cancels the line integral over C_∞. This is shown in Appendix A. Since the far-field intergrals over S_∞ and C_∞ cancel, we obtain

$$f_{ij}(U) - f_{ji}(-U) = i\sigma\rho \iint_{S_B} \left(\phi_j \frac{\partial \psi_i}{\partial n} - \psi_i \frac{\partial \phi_j}{\partial n}\right) dS = 0 \tag{4.15}$$

Thus, we have shown that the Timman-Newman relations are satisfied also in the case with the free surface condition (2.14) for a body of general shape.

The figures 4.1 and 4.2 illustrate the validity of the Timman-Newman relations for a half-immersed sphere at Froude number $Fr = 0.04$. The surge-heave and heave-surge hydrodynamic coefficients are zero at $Fr = 0$, so at small forward speed they are essentially proportional to Fr. The differences between the surge-heave and heave-surge coefficients at $Fr = \pm 0.04$ are at most 2% for the added mass and 7% for the damping coefficients.

From the Timman-Newman relations (4.4), we obtain the following symmetry relations for the diagonal entries of the added-mass and damping tensors:

$$f_{ii}(U) = f_{ii}(-U) \tag{4.16}$$

and thus we have

$$\left[\frac{\partial f_{ii}}{\partial U}\right]_{U=0} = 0 \tag{4.17}$$

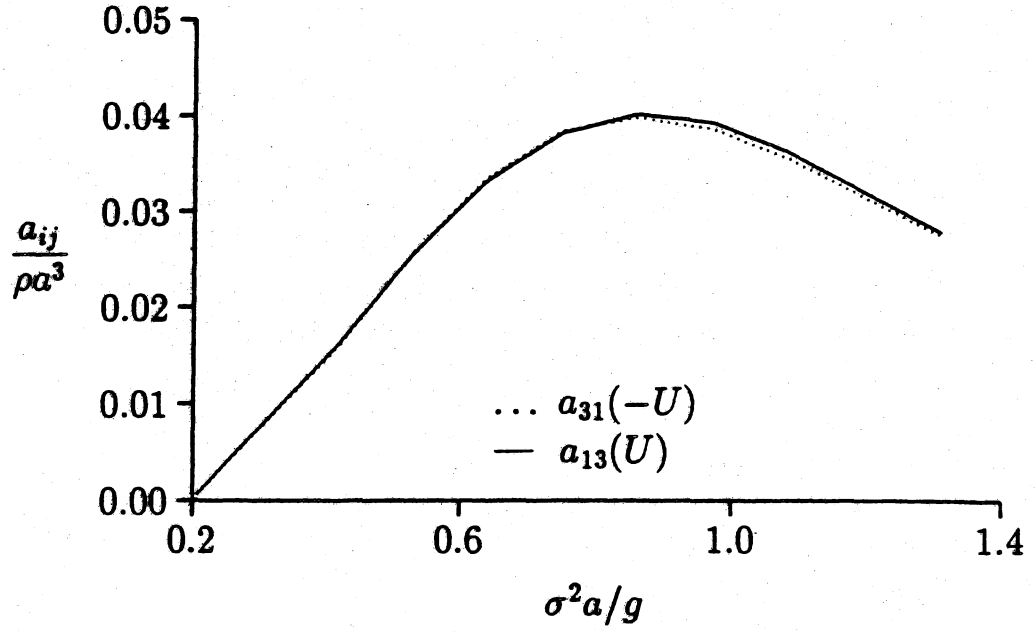

Figure 4.1: Cross-coupling added-mass coefficients a_{13} and a_{31} for a half-immersed sphere of radius a at $Fr = \pm 0.04$.

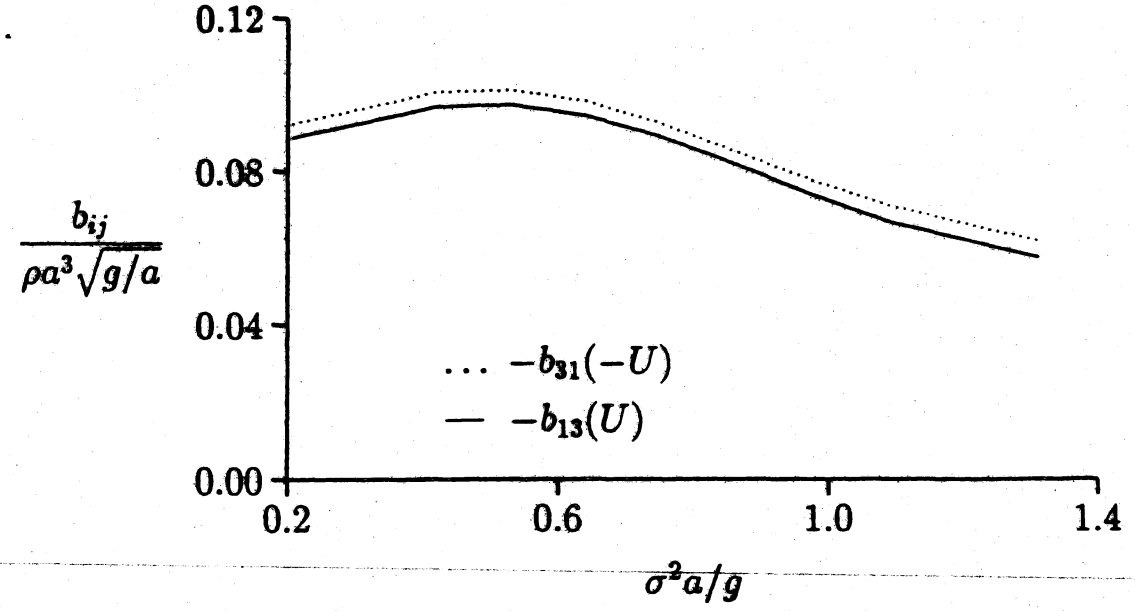

Figure 4.2: Cross-coupling damping coefficients b_{13} and b_{31} for a half-immersed sphere of radius a at $Fr = \pm 0.04$.

Therefore the Taylor expansion of $f_{ii}(\tau)$ about $\tau = 0$ may be written on the form

$$f_{ii}(\tau) = f_{ii}(0) + \mathcal{O}(\tau^2) \tag{4.18}$$

Thus, to leading order the added mass and damping coefficients are independent of τ. This is confirmed by the numerical results.

From energy conservation, the mean work done by the damping force over one cycle is equal to the mean energy flux at infinity. Therefore the damping coefficients can be related to the amplitude distributions $H_j(\theta)$ of the radiation potentials in the far-field. By using the far-field Haskind relations (4.28) derived in the next section, it is possible to express the diagonal damping coefficients as an integral of the corresponding exciting force coefficients squared over all wave incidence angles. However, since the diagonal damping coefficients are independent of τ to leading order, they can be found from the Haskind-Newman relations (Newman, 1977), which relate the zero-Froude number damping coefficients and exciting forces to each other. Thus, the diagonal damping coefficients can be obtained to first order in τ from the zero Froude number diffraction potential.

4.2 The exciting forces

The Haskind relations express the exciting force in terms of the incident-wave potential ϕ_0 and the reversed-flow radiation potentials ψ_i, so that the first-order exciting forces can be computed without knowing the scattering potential ϕ_7. The Haskind relations for zero forward speed have been known for a long time, see for example Newman (1977). The generalized Haskind relations including small forward speed have been derived by Zhao and Faltinsen (1987) for the two-dimensional case. We will derive the Haskind relations with forward speed for the three-dimensional case, and simplify them by exploiting the fact that the incident-wave potential satisfies the free surface condition (2.15). At last we will use Green's theorem to rewrite the Haskind relations into a form only involving integrals over the far-field. Using the far-field behaviour of the radiation potentials will then give us the far-field Haskind relations on a very convienient form. The diffraction force and moment is given as

$$F_i = -\rho \iint_{S_B} \left(\frac{\partial \phi_D}{\partial t} + \nabla \phi_s \cdot \nabla \phi_D \right) dS \tag{4.19}$$

where $i = 1, \ldots, 6$, and ϕ_D is the total diffraction potential given by (2.5). Inserting (2.5) and applying Tuck's theorem (2.33), the force and moment may be written

$$F_i = \mathrm{Re}\left(A e^{i\omega t} X_i \right) \tag{4.20}$$

where the exciting force coefficients X_i are given as

$$X_i = -i\sigma\rho \iint_{S_B} (\phi_0 + \phi_7) \frac{\partial \psi_i}{\partial n} dS \tag{4.21}$$

where ψ_i denotes the reversed-flow radiation potentials defined by (4.5) and (4.6). Applying Green's theorem to ϕ_7 and ψ_i, we find that

$$\iint_{S_B+S_F+S_\infty} \left(\phi_7 \frac{\partial \psi_i}{\partial n} - \psi_i \frac{\partial \phi_7}{\partial n} \right) dS = 0 \tag{4.22}$$

Using the free surface condition (2.14) on $\phi_0 + \phi_7$, we have that the free surface integral can be written

$$\iint_{S_F} \left(\phi_7 \frac{\partial \psi_i}{\partial n} - \psi_i \frac{\partial \phi_7}{\partial n} \right) dS =$$

$$2i\tau \iint_{S_F} \nabla_1 \cdot (\phi_7 \psi_i \nabla_1 \chi_s)\, dS + 2i\tau \iint_{S_F} \psi_i \left(\nabla_1 \phi_0 \cdot \nabla_1 \chi + \frac{1}{2} \phi_0 \nabla_1^2 \chi \right) dS \tag{4.23}$$

The first integral can be rewritten using Gauss' theorem, resulting in a line integral over C_∞ that cancels the surface integral over S_∞, as shown in Appendix A. This is in complete analogy to the proof of the Timman-Newman relations. Inserting (4.23) and the body boundary condition (2.9) into (4.22), we obtain

$$\iint_{S_B} \phi_7 \frac{\partial \psi_i}{\partial n} dS = - \iint_{S_B} \psi_i \frac{\partial \phi_0}{\partial n} dS - 2i\tau \iint_{S_F} \psi_i \left(\nabla_1 \phi_0 \cdot \nabla_1 \chi + \frac{1}{2} \phi_0 \nabla_1^2 \chi \right) dS \tag{4.24}$$

Inserting this into equation (4.21) for the exciting forces, we arrive at the Haskind relations

$$X_i = -i\sigma\rho \iint_{S_B} \left(\phi_0 \frac{\partial \psi_i}{\partial n} - \psi_i \frac{\partial \phi_0}{\partial n} \right) dS - 2\sigma\tau\rho \iint_{S_F} \psi_i (\nabla_1 \phi_0 \cdot \nabla_1 \chi + \frac{1}{2} \phi_0 \nabla_1^2 \chi) dS \tag{4.25}$$

Thus, the exciting forces can be obtained as an integral of the incident-wave potential and the reversed-flow radiation potentials over the body and the free surface.

It is also useful to rewrite the Haskind relations into a form only containing integrals over the far-field. By applying Green's theorem to ψ_i and ϕ_0, we can easily write the Haskind relations in the alternative form

$$X_i = i\sigma\rho \iint_{S_\infty} \left(\phi_0 \frac{\partial \psi_i}{\partial n} - \psi_i \frac{\partial \phi_0}{\partial n} \right) dS + 2\sigma\tau\rho \int_{C_\infty} \phi_0 \psi_i dy \tag{4.26}$$

This expression is especially convenient when the amplitude distributions of the radiation potentials are known.

To express the exciting force by the amplitude distribution $H_i(\theta; -\tau)$ of the reversed-flow radiation potentials ψ_i, we now introduce the expressions (4.14) for ψ_i and (2.6) for ϕ_0. Integrating with respect to z, we obtain

$$X_i = i\rho g \frac{\sigma}{\omega} \int_0^{2\pi} \left(\frac{k_1^-(\theta) - K\cos(\theta - \beta)}{k_1^-(\theta) + K} + 2\tau \cos\theta \right) e^{-i(K\cos(\theta-\beta) + k_1^-(\theta))R} R^{1/2} d\theta \tag{4.27}$$

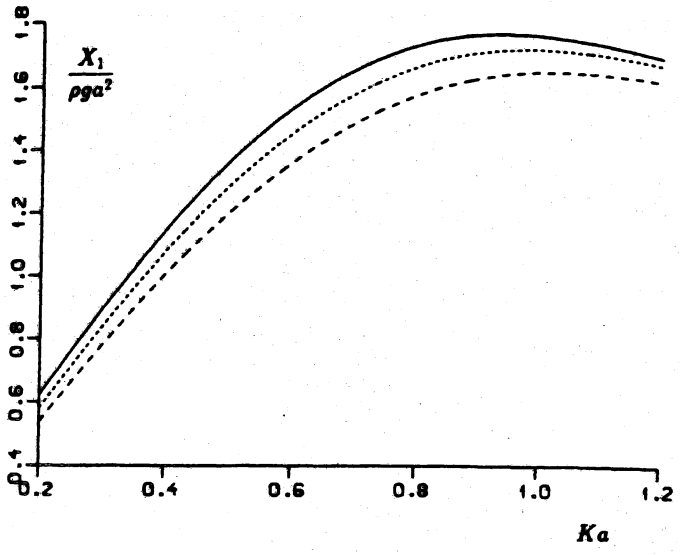

Figure 4.3: Surge exciting force X_1 for a half-immersed sphere of radius a in head waves and $Fr = 0, \pm 0.04$.

where $k_1^-(\theta)$ means $k_1(\theta; -\tau)$, and $R \to \infty$. Applying the method of stationary phase to the integral over θ, we finally obtain

$$X_i = \rho g \sqrt{\frac{2\pi}{K}}(1 - 2\tau \cos\beta) H_i(\beta + \pi + 2\tau \sin\beta; -\tau) e^{i\pi/4} + \mathcal{O}(\tau^2) \qquad (4.28)$$

where $H_i(\theta; \tau)$ is the amplitude distribution of the ith radiation potential, which is given by (4.13). Thus, the exciting force with forward speed can be found by evaluating the radiation potential far-field amplitude at one spatial angle, just as in the zero-speed case.

Figs. 4.3 and 4.4 show calculations of the exciting forces for a half-immersed sphere in head waves and $Fr = 0, \pm 0.04$. The far-field Haskind relations (4.28) are used. We see that the surge exciting force always increases with the Froude number, while the heave exciting force decreases with the Froude number for long waves and increases with the Froude number for short waves. In general, the influence of the forward speed upon the exciting forces is weaker than the influence upon the drift force, as shown in Fig. 5.1.

Figs. 4.5 and 4.6 show the derivatives of the exciting forces with respect to the forward speed computed by numerical differentiation of the data in Figs. 4.3 – 4.4. The method of direct pressure integration is compared to the far-field Haskind relations (4.28). The agreement between the two methods is excellent.

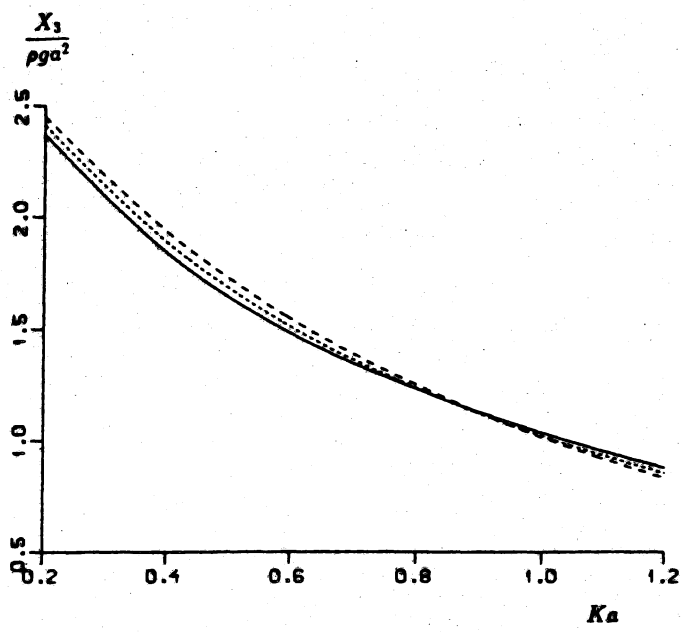

Figure 4.4: Heave exciting force X_3 for a half-immersed sphere of radius a in head waves and $Fr = 0, \pm 0.04$.

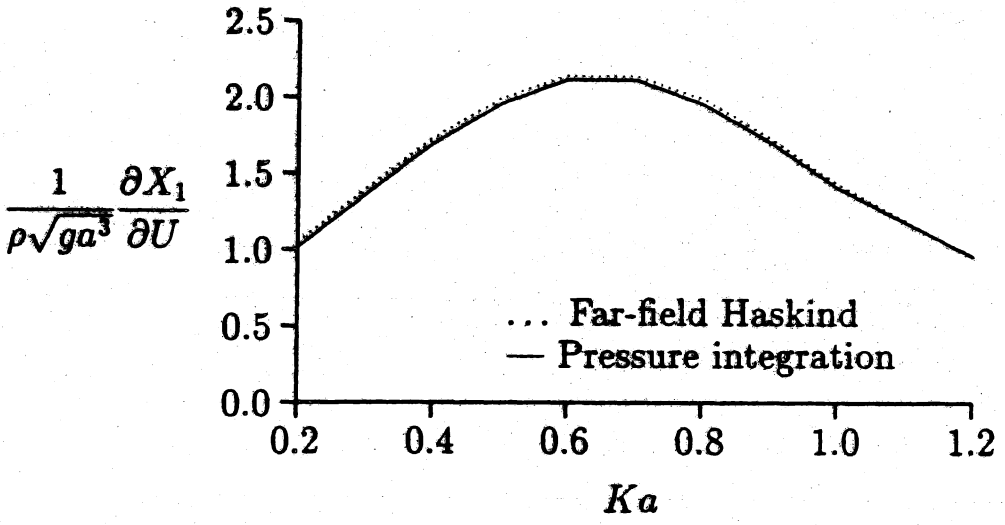

Figure 4.5: Derivative of the surge exciting force with respect to U for a half-immersed sphere of radius a in head waves. Comparison of near-field and far-field calculations.

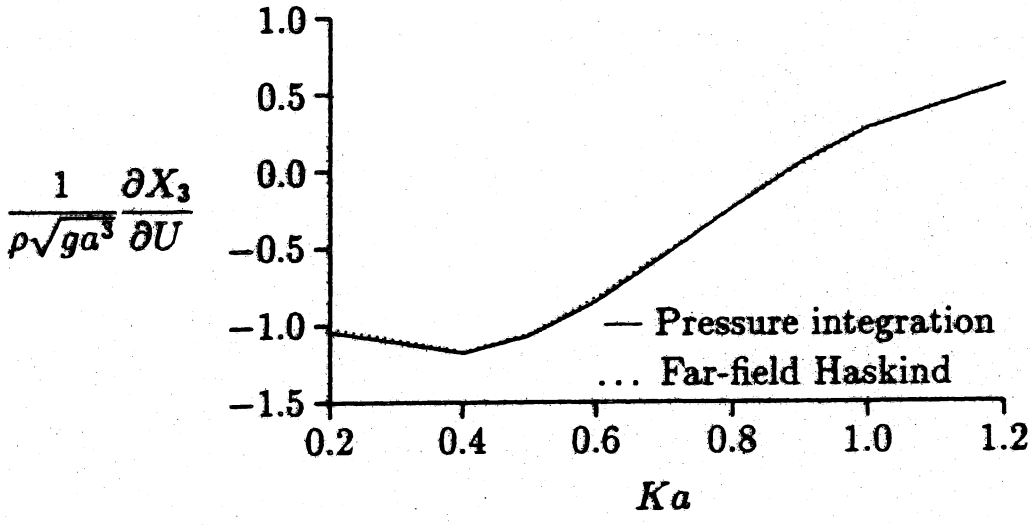

Figure 4.6: Derivative of the heave exciting force with respect to U for a half-immersed sphere of radius a in head waves. Comparison of near-field and far-field calculations.

Chapter 5

The drift force and the energy equation

In this section we will show how to compute the wave drift force from far-field analysis and check the energy conservation in the diffraction problem.

First we need the asymptotic expansions of the radiation and scattering potentials for large distances from the origin. The total diffraction potential is given by (2.5). For $R \to \infty$, the scattering potential ϕ_7 is given by

$$\phi_7 = R^{-1/2}\frac{ig}{\omega}H_7(\theta)e^{k_1 z - ik_1 R} + \mathcal{O}(\tau^2) \tag{5.1}$$

where $H_7(\theta)$ is the amplitude distribution of the scattering potential, and the wave number k_1 is given by

$$k_1 = \nu(1 + 2\tau\cos\theta) + \mathcal{O}(\tau^2) \tag{5.2}$$

The amplitude distribution $H_7(\theta)$ of the scattering potential ϕ_7 is obtained by inserting (5.1) and the far-field expansion (3.19) of the Green function into the integral equations (2.27). This yields

$$H_7(\theta) = \iint_{S_B}\phi\frac{\partial h}{\partial n}dS - 2i\tau\iint_{S_F}\phi(\nabla_1 h\cdot\nabla_1\chi + \frac{1}{2}h\nabla_1^2\chi)dS \tag{5.3}$$

where $\phi = \phi_0 + \phi_7$,

The total radiation potential is given by (2.4). For $R \to \infty$, the radiation potentiala ϕ_j is given by

$$\phi_j = R^{-1/2}H_j(\theta)e^{k_1 z - ik_1 R} + \mathcal{O}(\tau^2) \tag{5.4}$$

for $j = 1, \ldots, 6$, where $H_j(\theta)$ are given by (4.13).

5.1 The mean drift force

We now want to compute the mean drift force along the current direction. We want to avoid direct pressure integration, which is less accurate than far-field methods. To derive an expression for the drift force, we apply the momentum equation to the entire fluid domain. The mean drift force on the body must be equal to the mean flux of momentum into the fluid domain minus the mean force on a control suface at infinity. Since the steady disturbance $\chi(\boldsymbol{x})$ behaves as a dipole at large distances from the body, the velocity potential for $R \to \infty$ is written $\Phi(\boldsymbol{x}) - Ux$, where Φ is the total wave disturbance. Thus, the x component of the mean force must be

$$\overline{F_x} = \rho \int_0^{2\pi} \overline{\int_{-\infty}^{\zeta} \left[\left(\frac{\partial \Phi}{\partial x} - U \right) \left(\frac{\partial \Phi}{\partial R} - U\cos\theta \right) - p\cos\theta \right] dz R d\theta} \tag{5.5}$$

where $R \to \infty$. An overbar denotes the average with respect to time. The pressure p is given by the Bernoulli equation, and $z = \zeta(x,y)$ denotes the free surface elevation. $\zeta(x,y)$ is given by the dynamic free surface condition, which, since χ is negligible for large R, attains the form

$$\frac{\partial \Phi}{\partial t} - U\frac{\partial \Phi}{\partial x} + \frac{1}{2}|\nabla\Phi|^2 + g\zeta = 0 \text{ on } z = 0 \tag{5.6}$$

Since mass is conserved, the mean mass flux across the control surface at infinity must be zero, that is,

$$\rho \int_0^{2\pi} \overline{\int_{-\infty}^{\zeta} \left(\frac{\partial \Phi}{\partial R} - U\cos\theta \right) dz R d\theta} = 0 \tag{5.7}$$

Integrating the momentum equation (5.5) with respect to z and using the continuity equation (5.7), we obtain the following expression for the mean wave drift force in forward speed direction:

$$\overline{F_x} = \rho \int_0^{2\pi} \left\{ -\frac{1}{2g} \left[\overline{\left(\frac{\partial \Phi}{\partial t} \right)^2} - U^2 \overline{\left(\frac{\partial \Phi}{\partial x} \right)^2} \right]_{z=0} \cos\theta + \int_{-\infty}^{0} \left[\frac{1}{2}\overline{|\nabla\Phi|^2}\cos\theta - \overline{\frac{\partial \Phi}{\partial x}\frac{\partial \Phi}{\partial R}} \right] dz \right\} R d\theta \tag{5.8}$$

To obtain a momentum equation more suitable for numerical computation, we insert $\Phi = \mathrm{Re}\{\frac{iAg}{\omega}\phi e^{i\sigma t}\}$ into (5.8). Averaging with respect to time, we find the equation

$$\frac{\overline{F_x}}{\rho g A^2} = -\frac{1}{4}\int_0^{2\pi} \left\{ \frac{\sigma^2}{\omega^2}|\phi|^2\cos\theta - \frac{1}{K}\int_{-\infty}^{0} \left[|\nabla\phi|^2\cos\theta - 2\mathrm{Re}\frac{\partial \phi}{\partial x}\frac{\partial \phi^*}{\partial R} \right] dz \right\} R d\theta \tag{5.9}$$

where ϕ is defined by

$$\frac{iAg}{\omega}\phi = \phi_0 + \phi_7 + i\sigma\sum_{j=1}^{6}\xi_j\phi_j \tag{5.10}$$

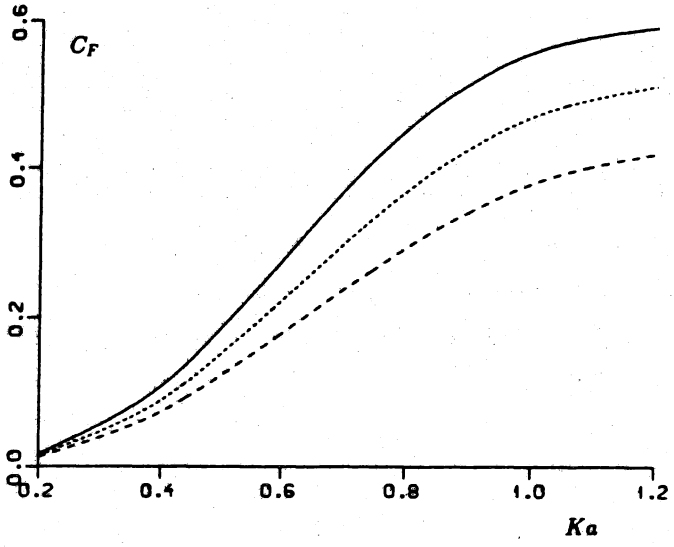

Figure 5.1: Mean drift force on a half-immersed sphere of radius a in head waves and $Fr = 0, \pm 0.04$.

We now insert the expressions (2.6) for ϕ_0, (5.1) for the scattering potential ϕ_7 and (5.4) for the radiation potentials ϕ_j. Using the method of stationary phase gives us the wave drift force as

$$\frac{\overline{F_x}}{\rho g A^2} = -\frac{1}{4}\left\{\int_0^{2\pi} B(\theta)|H(\theta)|^2 d\theta + 2\cos\beta(1 - 2\tau\cos\beta)S\right\} + \mathcal{O}(\tau^2) \tag{5.11}$$

where

$$B(\theta) = (1 - 2\tau\cos\beta)\cos\theta + 2\tau\sin^2\theta$$

$$S = \sqrt{\frac{2\pi}{\nu}}\,\mathrm{Re}\left(e^{i\pi/4}H^*(\beta + 2\tau\sin\beta)\right) \tag{5.12}$$

$$H(\theta) = H_7(\theta) + \nu(1 + \tau\cos\beta)\sum_{j=1}^{6}\frac{\xi_j}{A}H_j(\theta)$$

where $H_j(\theta)$ is given by (5.1) - (5.4).

Fig. 5.1 shows the mean drift force in head waves ($\beta = \pi$) at $Fr = 0, \pm 0.04$. The sphere is restrained from moving in first-order motions. As this figure shows, the influence of forward speed is much stronger on the drift force than on the first order forces.

5.2 The energy equation

To check the numerical results, it is useful to have an energy equation. Let us consider energy conservation for the diffraction problem. For a fixed body, the energy flux across a vertical cylinder of large radius must be zero in the mean. The energy flux across the cylinder is given by

$$W = \rho \int_0^{2\pi} \overline{\int_{-\infty}^{\zeta} \left(p + \frac{1}{2}|\nabla\phi_D|^2 + gz\right)\left(\frac{\partial\phi_D}{\partial R} - U\cos\theta\right) dz R d\theta} \tag{5.13}$$

where $z = \zeta$ denotes the free surface elevation given by (5.6). We now insert the pressure p from the Bernoulli equation and use the equation (5.6) for the free surface elevation. Integrating with respect to z, we obtain

$$W = -\rho \int_0^{2\pi} \left\{ \int_{-\infty}^{0} \overline{\frac{\partial\phi_D}{\partial t}\frac{\partial\phi_D}{\partial R}} dz + \frac{U\cos\theta}{g} \overline{\left[\frac{\partial\phi_D}{\partial t}\left(\frac{\partial\phi_D}{\partial t} - U\frac{\partial\phi_D}{\partial x}\right)\right]_{z=0}} \right\} R d\theta \tag{5.14}$$

where Φ_D means the total diffraction potential (2.5). Proceeding as in the previous section, we insert $\Phi = \mathrm{Re}\{\frac{iAg}{\omega}\phi e^{i\sigma t}\}$ into (5.14) and take the average with respect to time. This yields

$$\frac{W}{\rho g A^2 \sigma/2K} = -\int_0^{2\pi} \left\{ \tau\cos\theta|\phi|^2 + \int_{-\infty}^{0} \mathrm{Re}\,(i\phi\frac{\partial\phi^*}{\partial R}) dz \right\} R d\theta \tag{5.15}$$

We now introduce the expressions (2.6) for ϕ_0 and (5.1) for ϕ_7 and use the method of stationary phase. Then we require that the energy be conserved, which means that $W = 0$. This yields

$$\int_0^{2\pi} A(\theta)|H_7(\theta)|^2 d\theta - (1 - 2\tau\cos\beta)S = \mathcal{O}(\tau^3) \tag{5.16}$$

where

$$A(\theta) = \tau\cos\theta - \frac{1}{2} \tag{5.17}$$

and S is given by (5.12).

The energy equation (5.16) for the diffraction problem can be used to simplify the expression for the wave drift force for a fixed body. Eliminating the stationary phase term S from (5.16) and inserting this into the momentum equation (5.11) yields the following alternative expression for the mean drift force for a fixed body:

$$\frac{\overline{F_x}}{\rho g A^2} = -\frac{1}{4}\int_0^{2\pi} \left(\cos\theta - \cos\beta + 2\tau\sin^2\theta\right)|H_7(\theta)|^2 d\theta + \mathcal{O}(\tau^2) \tag{5.18}$$

Comparing the drift force equations (5.11) and (5.18) may give an idea of the degree of energy conservation in the method. Fig. 5.2 shows the mean drift force in head waves at

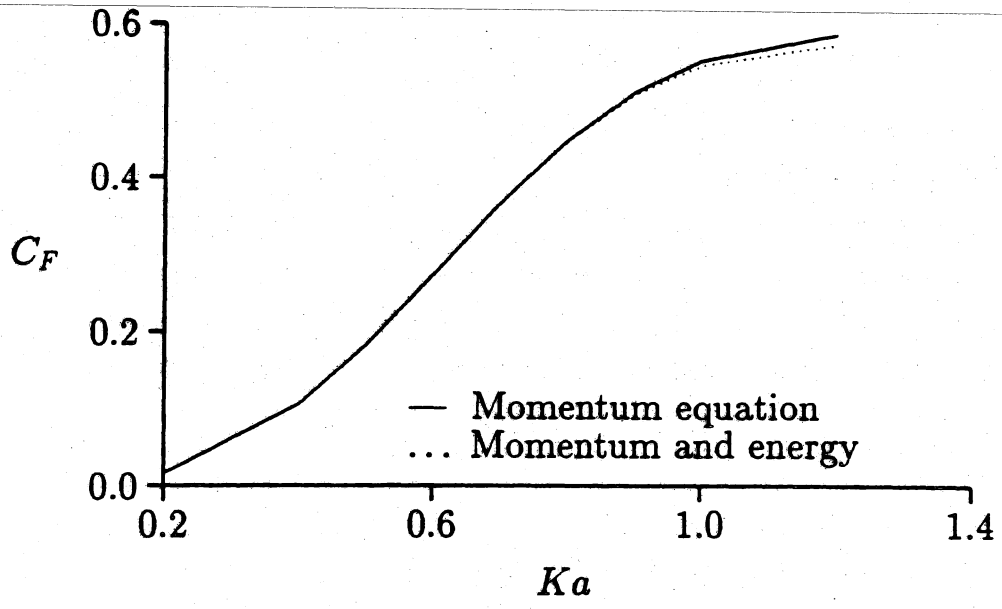

Figure 5.2: Mean drift force on a half-immersed sphere of radius a in head waves and $Fr = 0.04$. Comparison of momentum and momentum/energy computations.

$Fr = 0.04$. The results from the momentum equation (5.11) and the combined momentum and energy equation (5.18) are compared. The maximum deviation is 2%, which indicates satisfying energy conservation. Since the error is quadratic in Fr, doubling the Froude number to 0.08 gives a deviation of about 8%.

Chapter 6

Discussion of results

In this chapter we present some numerical examples and comparisons with other authors' results. Results for three different geometries are given: A half-immersed sphere, a truncated vertical surface-piercing cylinder and an array of vertical truncated cylinders.

6.1 The half-immersed sphere

The first example is a half-immersed sphere of radius a. The body has been discretized with 200 panels on half of the wetted surface. The free surface has been discretized out to a radius of $6a$, with 440 panels on the halfplane $z = 0$, $y > 0$. The results presented are for $Fr = 0.03$, where the Froude number is given by

$$Fr = \frac{U}{\sqrt{ga}}$$

Computations of the cross-coupling added mass and damping coefficients, linear exciting force and wave drift force along the current direction (for $Fr = 0.04$) have been shown in the two previous chapters. Figs. 6.1 – 6.4 show convergence tests for the half-immersed sphere. The computed values of the surge exciting force and the drift force change by about 2% when the number of panels on half the wetted surface is increased by a factor of 8, from 50 to 400. Curiously, the heave exciting force converges unusually fast. This might be related to the fact that the agreement between pressure integration and the Haskind relations is especially good for the heave exciting force. Some kind of cancellation of numerical errors seems to occur. The convergence of the drift force is as good for the freely moving cylinder in Fig. 6.4 as for the restrained one in Fig. 6.3, indicating that the radiation and diffraction potentials are about equally accurate for the sphere.

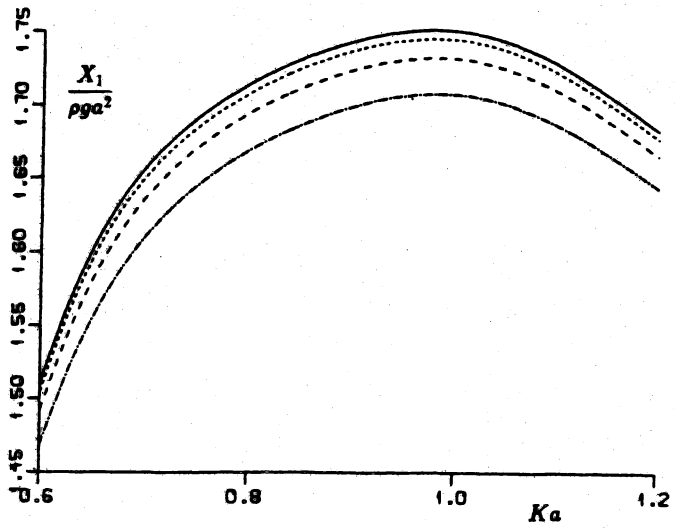

Figure 6.1: Convergence of the surge exciting force for a half-immersed sphere in head waves and $Fr = 0.03$.

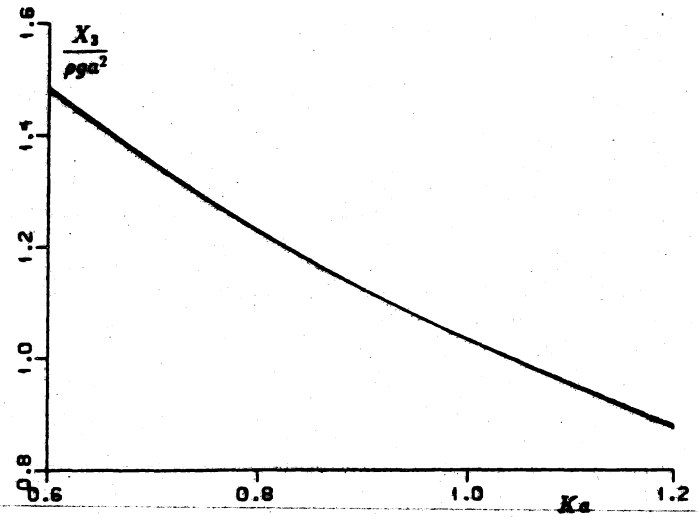

Figure 6.2: Convergence of the heave exciting force for a half-immersed sphere in head waves and $Fr = 0.03$.

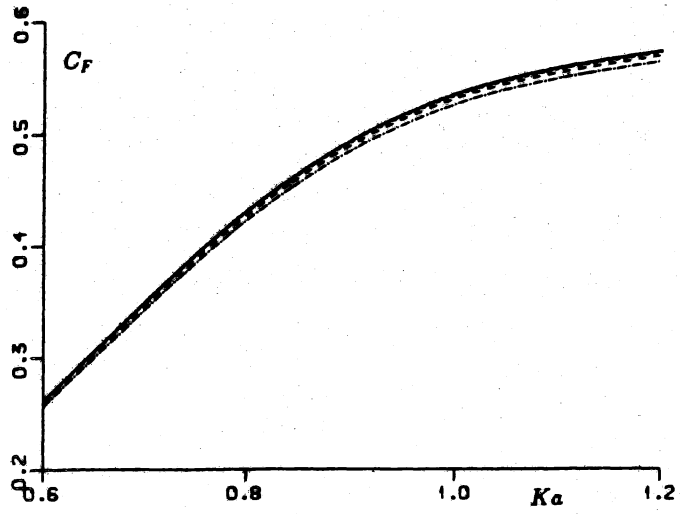

Figure 6.3: Convergence of the wave drift force for a restrained half-immersed sphere in head waves and $Fr = 0.03$.

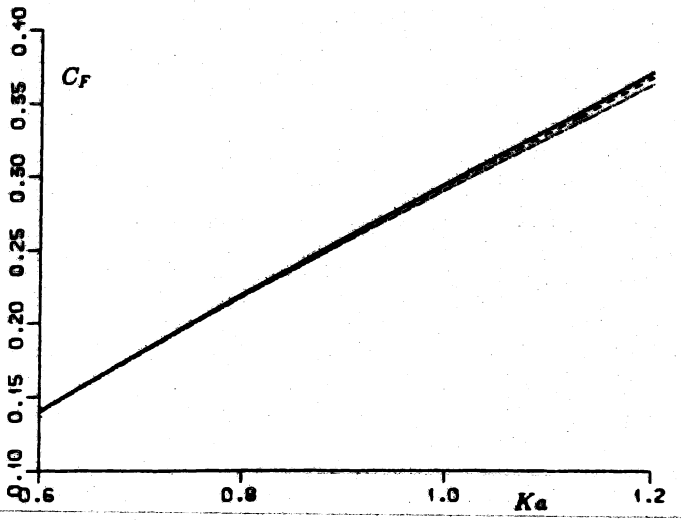

Figure 6.4: Convergence of the wave drift force for a half-immersed sphere free to surge in linear motion in head waves and $Fr = 0.03$.

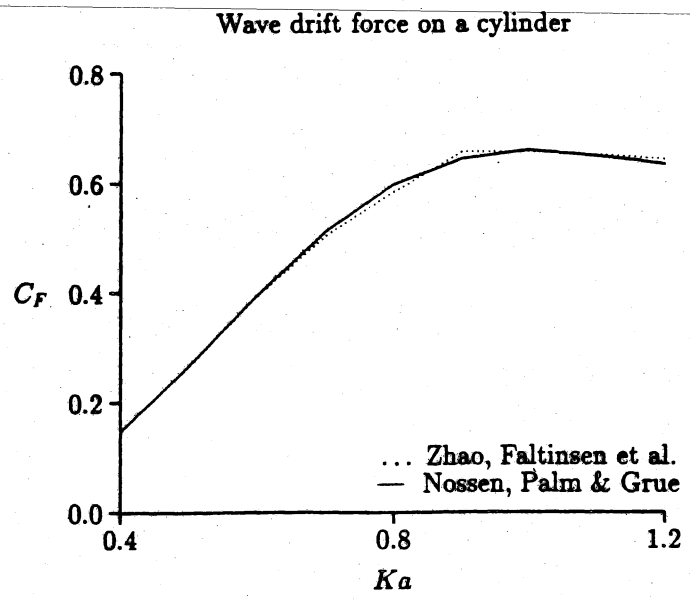

Figure 6.5: Mean drift force on a restrained floating cylinder of radius a and draft $3a$ in head waves and $Fr = 0$. Comparison between the present method and that of Zhao and Faltinsen.

6.2 The vertical cylinder

The second example is a vertical surface-piercing circular cylinder of radius a and draft $3a$. The body has been discretized with 280 panels on half of the wetted surface. The free surface has been discretized out to a radius of $6a$, with 224 panels on the halfplane $z = 0$, $y > 0$.

Fig. 6.5 shows a comparison of the drift force at $Fr = 0$ compared to the results of Zhao and Faltinsen (1989). The drift force coefficient is defined by

$$C_F = \frac{\overline{F_x}}{\rho g A^2 a}$$

The cylinder is restrained from moving in first-order motions. The agreement is very good, with a maximum discrepancy of about 2%.

Fig. 6.6 shows a comparison of the corresponding wave drift damping. The wave drift damping is obtained here by evaluating the drift force at $Fr = \pm 0.0319$. and using numerical differentiation. There is some discrepancy at the higher frequencies, up to about 18% in the worst case. Some of this discrepancy may be due to differences in the methods, since the method of Zhao and Faltinsen includes some nonlinear forward speed effects in the Green function. At lower frequencies, the agreement is excellent.

Fig. 6.7 shows the mean drift force on the cylinder at $Fr = 0.0226$ in head waves when the cylinder is free to surge in linear motion, but restrained in the other modes of motion.

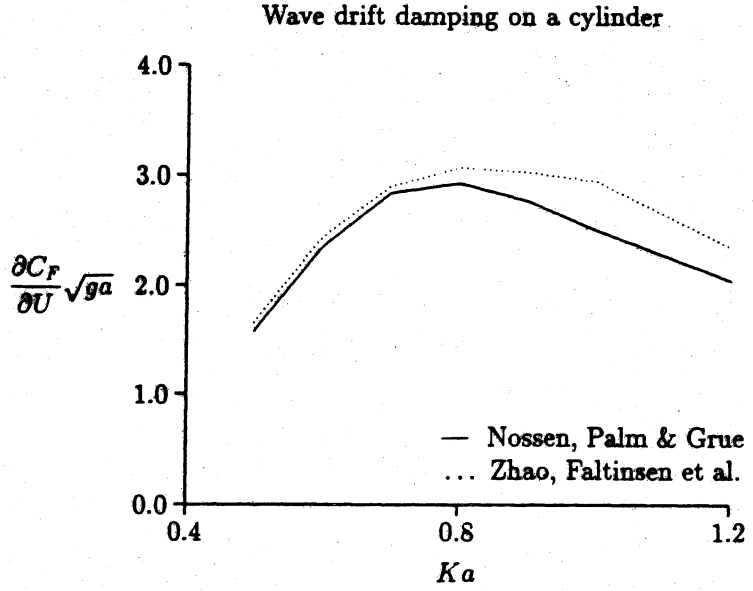

Figure 6.6: Wave drift damping on a restrained floating cylinder of radius a and draft $3a$ in head waves. Comparison between the present method and that of Zhao and Faltinsen.

The maximum difference in the results between the present theory and that of Zhao and Faltinsen is about 5%. For the lower frequencies, the results are almost indistinguishable.

Fig. 6.8 shows the corresponding wave drift damping, obtained by numerical differentiation of the drift force at $Fr = \pm 0.0226$. Surprisingly, the agreement is better than for the restrained cylinder. The slightly lower Froude number is not enough to explain this feature. The calculations differ by up to 10% at the higher frequencies. Some of this might possibly be due to different treatment of the m-terms. Still, a disagreement of 10% is not much, taking into account that the wave drift damping is computed by numerical differentiation. The agreement at low frequencies is again very good.

Figs. 6.9 – 6.11 show convergence of the surge exciting force and the wave drift force for the cylinder at $Fr = 0.03$. The far-field Haskind relations (4.28) are used for the exciting force. The cylinder is restrained in Fig. 6.10 and free to surge in linear motion in Fig. 6.11. For the exciting force, the rate of convergence is about the same as for the half-immersed sphere. Also for the restrained cylinder in Fig. 6.10, the drift force converges as fast as for the sphere in Fig. 6.3. When the bodies are free to move in surge, the convergence seems to be slightly slower for the cylinder in Fig. 6.11 than for the sphere in Fig. 6.4. Since the convergence rate is the same for the two restrained bodies, it is likely that the inaccuracy in the drift force for the surging cylinder is caused by the singularity in the right-hand side of the radiation problem at the edge of the cylinder, as discussed earlier in Section 2.5. The convergence is still satisfying, with 200 panels on half of the wetted surface giving sufficient accuracy.

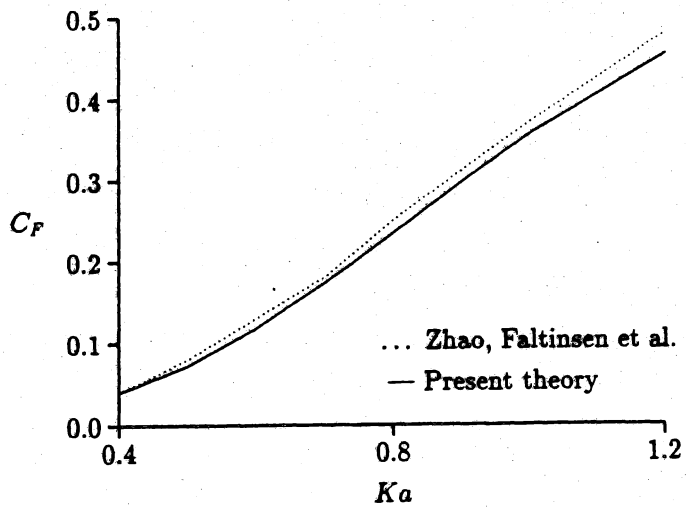

Figure 6.7: Mean drift force on a floating cylinder of radius a and draft $3a$ free to surge in head waves and $Fr = 0.0226$. Comparison between the present method and that of Zhao and Faltinsen.

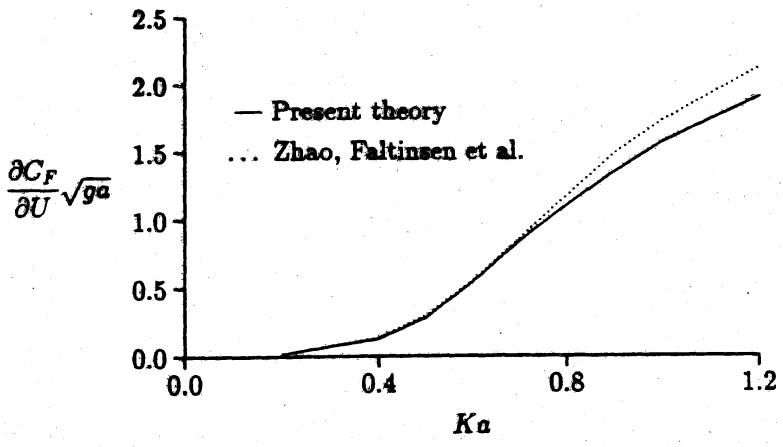

Figure 6.8: Wave drift damping on a floating cylinder of radius a and draft $3a$ free to surge in head waves. Comparison between the present method and that of Zhao and Faltinsen.

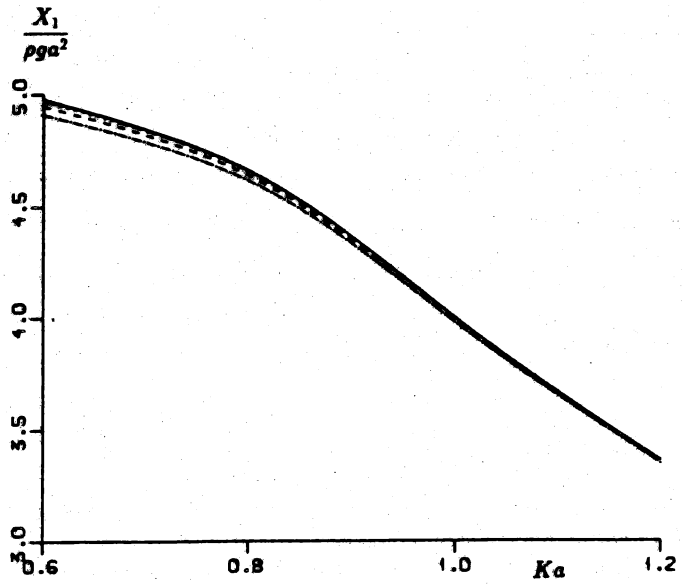

Figure 6.9: Convergence of the surge exciting force for a vertical cylinder in head waves and $Fr = 0.03$.

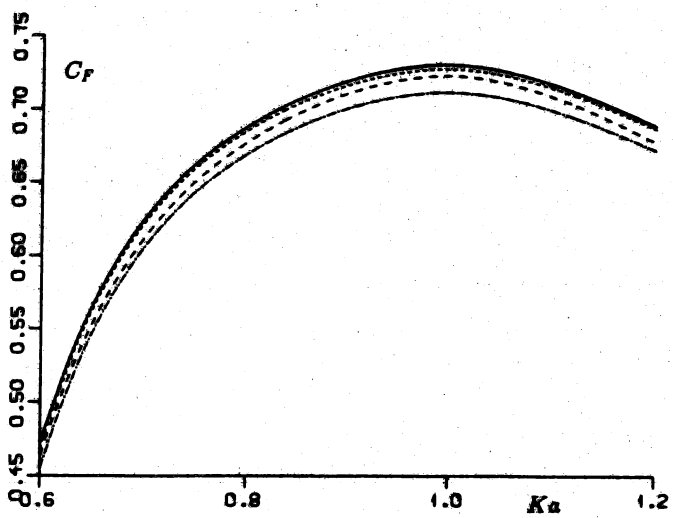

Figure 6.10: Convergence of the wave drift force for a restrained vertical cylinder in head waves. $Fr = 0.03$.

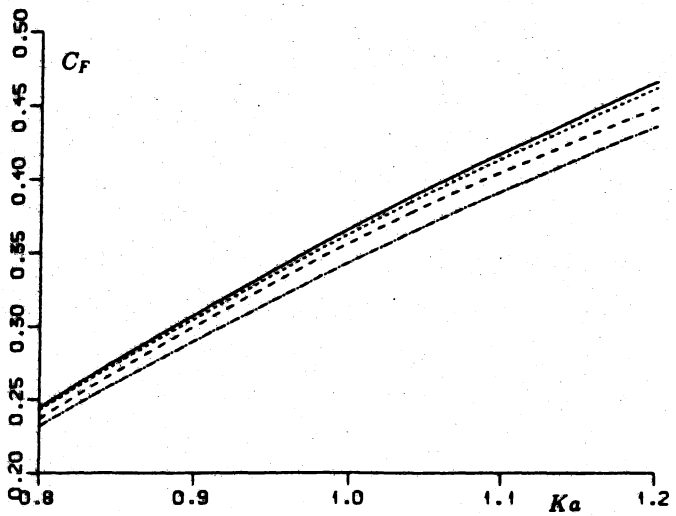

Figure 6.11: Convergence of the wave drift force for a vertical cylinder free to surge in linear motion in head waves. $Fr = 0.03$.

6.3 The array of vertical cylinders

The third example is an array of four vertical cylinders, each one identical to the one in the previous example, with radius a and draft $3a$. The centres of the cylinders generate a square with sides $7a$. This configuration, shown in Fig. 6.12, resembles the four corner columns of a tension-leg platform. The geometry is discretized with 192 panels on each column and with 468 panels on half of the free surface. The discretization of the free surface is shown in Fig. 6.13. Figure 6.14 shows the wave drift force for this geometry at zero forward speed, with typical interference phenomena acting between the different columns. As Fig. 6.14 shows, the mean drift force on each cylinder in the array may be considerably greater than the drift force on a single cylinder, which is given in Fig. 6.7. This is of course caused by the nonlinear interactions between the scattered and radiated waves from the different columns. Fig. 6.15 shows the corresponding wave drift damping. Due to interference phenomena, the wave drift damping oscillates quite rapidly and becomes negative at some frequencies. This means that the mean drift force decreases with increasing forward speed at these frequencies, while for a single column, the mean drift force always increases with increasing forward speed, as shown in Fig. 6.8. Thus, the interference between different structure members changes the behaviour of the wave drift damping radically. Remarkably, the frequency interval in which the wave drift damping is negative for the cylinder array is approximately the interval for which the wave drift force decreases with increasing frequency. This is not easy to interpret physically, but this

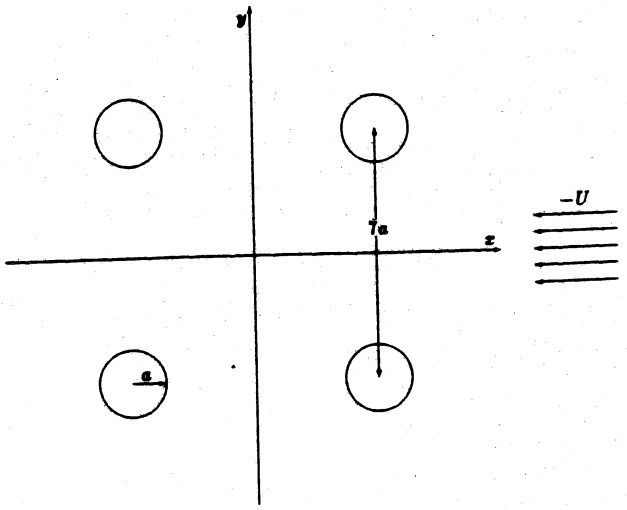

Figure 6.12: Geometry of cylinder array viewed from above.

interval ($0.5 < Ka < 0.7$) is clearly the interval in which the interaction between the columns has the most dramatic consequences.

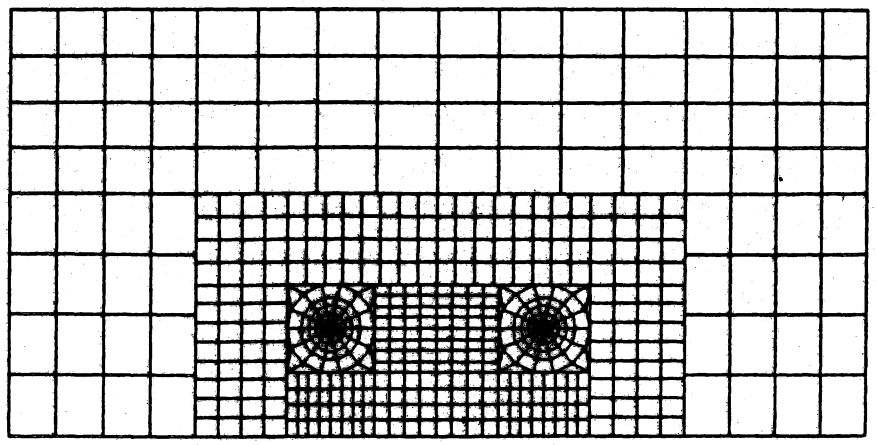

Figure 6.13: Discretization of the free surface around the cylinder array in the halfplane $y > 0$.

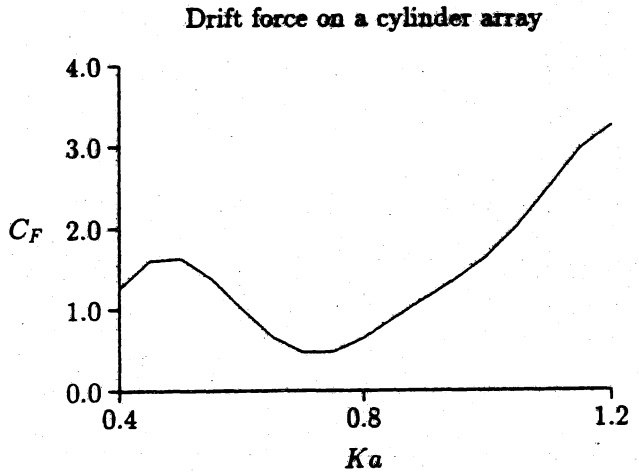

Figure 6.14: mean drift force on a floating cylinder array free to surge in head waves and $Fr = 0$. Cylinder radius a, draft $3a$, distance between centers $7a$.

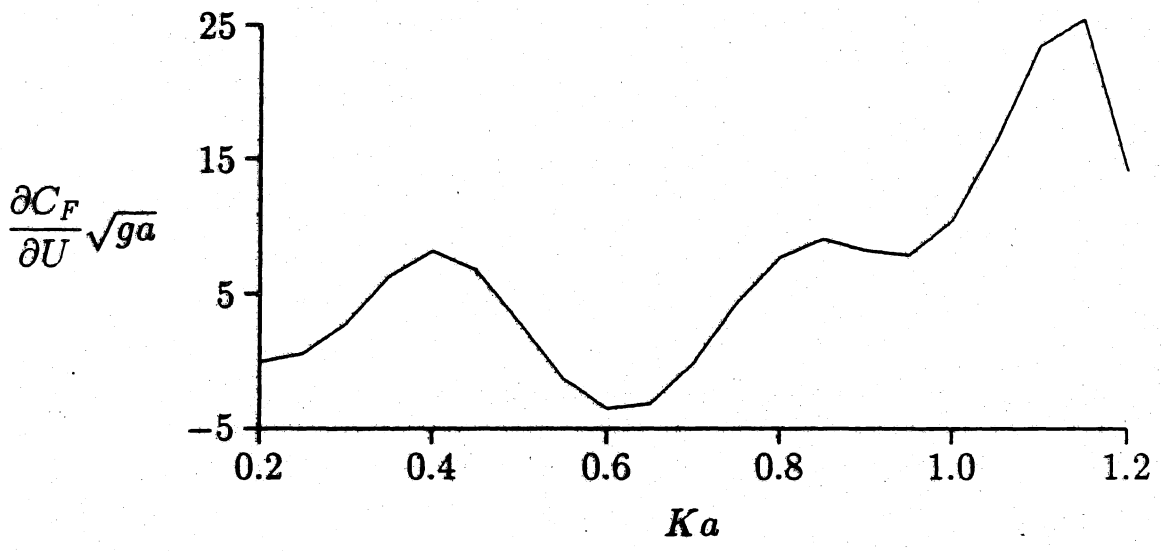

Figure 6.15: Wave drift damping on a floating cylinder array free to surge in head waves. Cylinder radius a, draft $3a$, distance between centers $7a$.

Chapter 7

Acknowledgements

Financial support for this work has been granted by the Royal Norwegian Council for Science and the Humanities (NAVF) and by Saga Petroleum A/S. The WAMIT radiation/diffraction program has been provided by Veritas Sesam Systems A/S.

Bibliography

[1] CHANG, M.S., Computations of three-dimensional ship motions with forward speed. *2nd Internat. Confer. on Numerical Ship Hydrodynamics*, 124-135, 1977.

[2] HASKIND, M.D., The hydrodynamic theory of ships oscillating in rolling and pitching. *Prikl. Mat. Mekh.* **10**, 1946, 33-66.

[3] HUIJSMANS, R.H.M. AND HERMANS, A.J., A fast algorithm for computation of 3-D ship motions at moderate forward speed. *4th Internat. Confer. on Numerical Ship Hydrodynamics*, 1985.

[4] INGLIS, R.B. AND PRICE, W.G., The influence of speed dependent boundary conditions in 3-D ship motion problems. *Internat. Shipbuilding Progr.* **28**, 1981, 22-29

[5] MARUO, H., The Drift of a Body Floating on Waves. *J. of Ship Res.* 1960, 1-10.

[6] NEWMAN, J.N., The damping and wave resistance of a pitching and heaving ship. *J. of Ship Res.* 1959, 1-19.

[7] NEWMAN, J.N., Marine Hydrodynamics. The MIT Press, Cambridge, MA 1977

[8] NEWMAN, J.N., The theory of ship motions. *Advances in Applied Mechanics* **18**, 1978, 221-280.

[9] NEWMAN, J. N., An expansion of the oscillatory source potential. *Appl. Ocean Res.* **6**, 1984,116-117.

[10] NEWMAN, J. N. AND SCLAVOUNOS, P. D., WAMIT User's Manual. MIT 1987.

[11] OGILVIE, T.F. AND TUCK, E.O., A rational strip theory of ship motions: part 1. Report No 013,The Department of Naval Architecture and Marine Engineering, The University of Michigan, College of Engineering, 1969.

[12] PETERS, A.S. AND STOKER, J.J., The motion of a ship, as a floating, rigid body in a seaway. *Comm. on pure and applied mathem.* **10**, 1957, 399-490.

[13] TIMMAN, R. AND NEWMAN, J.N., The coupled damping coefficients of a symmetric ship. *J. of Ship Res.* **5**, 1962, 1-7

[14] ZHAO, R. AND FALTINSEN, O.M., Interaction between waves and current on a 2-D body in the free surface. *Appl. Ocean Res.* **10**, 1988, 87-99.

[15] ZHAO, R. AND FALTINSEN, O.M., Interaction between current, waves and marine structures. *5th International Confer. on Numerical Ship Hydrodynamics*,1989.

Appendix A

The far-field terms in the integral equations

We will now proceed to show that the integral expression in (2.25) vanishes. We then need the far-field behaviour of the Green function and the potentials, as in the section on the added mass and damping coefficients. Since we now integrate with respect to the source point coordinates, we need to replace the condition $|\boldsymbol{x}| \to \infty$ with $|\boldsymbol{\xi}| \to \infty$. This is accomplished by noting that

$$G(\boldsymbol{x}, \boldsymbol{\xi}; \tau) = G(\boldsymbol{\xi}, \boldsymbol{x}; -\tau) \tag{A.1}$$

Letting $\xi = R\cos\theta, \eta = R\sin\theta$ and using (3.19), the Green function for $R \to \infty$ can be written

$$G(R, \theta, \zeta; x, y, z) = R^{-1/2} h(\boldsymbol{x}, \theta; -\tau) e^{k_1(\theta;-\tau)(\zeta - iR)} \tag{A.2}$$

where $h(\boldsymbol{\xi}, \theta; \tau)$ is given by (3.20). From (5.1) – (5.4), we also have the far-field behaviour of the radiation and scattering potentials

$$\phi_j = R^{-1/2} H_j(\theta) e^{k_1(\theta;\tau)(\zeta - iR)}, \qquad j = 1, \ldots, 7 \tag{A.3}$$

where $R \to \infty$, and the amplitude distributions $H_j(\theta)$ are given by (4.13) – (5.3). Using these expressions and integrating with respect to ζ, we obtain

$$\iint_{S_\infty} \left(\phi_j \frac{\partial G}{\partial n} - G \frac{\partial \phi_j}{\partial n} \right) dS = 2i\tau e^{-2i\nu R} \int_0^{2\pi} H_j(\theta) h(\boldsymbol{x}, \theta; -\tau) \cos\theta d\theta \tag{A.4}$$

Similarly, we get

$$2i\tau \int_{C_\infty} \phi_j G d\eta = 2i\tau e^{-2i\nu R} \int_0^{2\pi} H_j(\theta) h(\boldsymbol{x}, \theta; -\tau) \cos\theta d\theta \tag{A.5}$$

which finally shows that

$$\iint_{S_\infty} \left(\phi_j \frac{\partial G}{\partial n} - G \frac{\partial \phi_j}{\partial n} \right) dS - 2i\tau \int_{C_\infty} \phi_j G d\eta = 0 \tag{A.6}$$

for $j = 1, \ldots, 7$. Thus, the far-field integrals in (2.23) and (2.24) cancel each other in both the radiation and diffraction problems.

A similar derivation is needed to prove the Timman-Newman relations (4.4). The far-field behaviour of the reversed-flow radiation potentials ψ_i is the same as (5.4), with the sign of τ reversed. This means that ψ_i plays a role similar to G in the far-field integrals over S_∞ and C_∞. Therefore we obtain, in analogy with (A.6),

$$\iint_{S_\infty} \left(\phi_j \frac{\partial \psi_i}{\partial n} - \psi_i \frac{\partial \phi_j}{\partial n} \right) dS - 2i\tau \int_{C_\infty} \phi_j \psi_i dy = 0 \tag{A.7}$$

which completes the proof of the Timman-Newman relations (4.4).

Appendix B

Application of Tuck's theorem to the source potential

In the formulation of the integral equations for the radiation potentials with forward speed, we have used Tuck's theorem in the form

$$\iint_{S_B} \nabla\chi_s(\xi) \cdot \nabla G^0(x,\xi) n_i dS_\xi = -\iint_{S_B} G^0(x,\xi) m_i dS_\xi \tag{B.1}$$

As stated previously, Tuck's theorem is clearly valid when x is outside the body, since $G^0(x,\xi)$ is differentiable for $x \neq \xi$. However, G is singular at $x = \xi$, so it's not obvious that Tuck's theorem can be applied when the field point is situated on the body.

But since G^0 itself is integrable, the right hand side in (B.1) is obviously continuous for $x \to S_B$. ∇G^0 is *not* integrable, but for any regular source distribution $Q(x)$ we have

$$\lim_{x \to S_B} \iint_{S_B} Q(\xi) \nabla G^0(x,\xi) dS_\xi = \frac{1}{2} Q(x) \mathrm{n} + \iint_{S_B} Q(\xi) \nabla G^0(x,\xi) dS_\xi \tag{B.2}$$

where the last integral is interpreted in a principal-value manner. Applying this result to (B.1), we have

$$\frac{1}{2} \nabla\chi_s \cdot \mathrm{n} + \iint_{S_B} \nabla\chi_s(\xi) \cdot \nabla G^0(x,\xi) n_i dS_\xi = -\iint_{S_B} G^0(x,\xi) m_i dS_\xi \tag{B.3}$$

Since $\partial\chi_s/\partial n = 0$, the residual contribution to the normal velocity drops out, and thus the left-hand side of (B.1) is also continuous $x \to S_B$, which means that Tuck's theorem is valid.

Appendix C

Numerical integration of the Green function

To solve the integral equations (2.31), (2.32) and (2.34) numerically, we need to integrate the Green functions (3.12) and (3.14) numerically over each panel. The integration of the zero-speed Green function (3.12) and its normal derivative is well documented in Newman and Sclavounos (1987). Here we will describe briefly how the forward speed Green function (3.14) and its normal derivative are integrated numerically.

Using the coordinates

$$\begin{aligned} R &= \sqrt{(x-\xi)^2+(y-\eta)^2} \\ r' &= \sqrt{(x-\xi)^2+(y-\eta)^2+(z+\zeta)^2} \\ \tan\theta &= \frac{y-\eta}{x-\xi} \end{aligned}$$

we find that (3.14) can be written

$$\begin{aligned} \psi_1 &= -4\pi\cos\theta\nu e^{\nu(z+\zeta)}\left[(1+\nu(z+\zeta))J_1(\nu R)+\nu R J_0(\nu R)\right] \\ &+ 4i\cos\theta[1+\nu(z+\zeta)]\frac{\partial I}{\partial R} - 4i\nu(x-\xi)\left(\frac{1}{r'}+\nu I\right) \end{aligned} \tag{C.1}$$

where the integral I is given by (3.13). The gradient of (3.14) with respect to the source point coordinates is given by

$$\begin{aligned} \frac{\partial\psi_1}{\partial\xi} &= 4\pi\nu^2 e^{\nu(z+\zeta)}\left[\frac{1}{2}(3+\nu(z+\zeta))J_0(\nu R)-\nu R\cos^2\theta J_1(\nu R)\right] \\ &+4\pi\nu^2 e^{\nu(z+\zeta)}\left[\frac{1}{2}(1+\nu(z+\zeta))(1-2\cos^2\theta)J_2(\nu R)\right] \\ &+4i\nu^2\left[\left(1+(1+\nu(z+\zeta))\cos^2\theta\right)I+\left(\frac{1+\nu(z+\zeta)}{\nu R}(1-2\sin^2\theta)+\nu R\cos^2\theta\right)\frac{\partial I}{\partial R}\right] \end{aligned}$$

$$+4i\nu^2\left[+(1+\nu(z+\zeta)\cos^2\theta)\frac{1}{\nu r'}+\cos^2\theta\frac{\partial}{\partial(\nu z)}\left(\frac{1}{\nu r'}\right)\right] \tag{C.2}$$

$$\frac{\partial\psi_1}{\partial\eta}=-4\pi\nu^2\cos\theta\sin\theta\ e^{\nu(z+\zeta)}\left[(1+\nu(z+\zeta))J_2(\nu R)+\nu RJ_1(\nu R)\right]$$
$$+4i\nu^2\cos\theta\sin\theta\left[(1+\nu(z+\zeta))I+\left(2\frac{1+\nu(z+\zeta)}{\nu R}+\nu R\right)\frac{\partial I}{\partial R}+\frac{z}{r'}+\frac{\partial}{\partial(\nu z)}\left(\frac{1}{\nu r'}\right)\right] \tag{C.3}$$

$$\frac{\partial\psi_1}{\partial\zeta}=-4\pi\nu^2\cos\theta\ e^{\nu(z+\zeta)}\left[(2+\nu(z+\zeta))J_1(\nu R)+\nu RJ_0(\nu R)\right]$$
$$+4i\nu^2\cos\theta\left[(2+\nu(z+\zeta))\frac{\partial I}{\partial R}-\nu RI-\frac{R}{r'}\right]+4i\frac{\partial}{\partial x}\left(\frac{1}{r'}\right) \tag{C.4}$$

Newman (1984) gives the integral I as an ascending series expansion in $X=\nu R$ and $Y=-\nu(z+\zeta)$. Using this series and its derivative, we find that the singular behaviours of I and its derivatives are

$$\begin{aligned} I &= -\ln\nu(r'+|z+\zeta|)+\mathcal{O}(1)\\ \frac{\partial I}{\partial R} &= -\frac{R}{r'(r'+|z+\zeta)}+\mathcal{O}(1)\\ \frac{1}{R}\frac{\partial I}{\partial R} &= -\frac{1+\nu r'}{r'(r'+|z+\zeta|)}+\frac{1}{2}\nu^2\ln\nu(r'+|z+\zeta|)+\mathcal{O}(1)\end{aligned} \tag{C.5}$$

To evaluate the integrals of ψ_1 and its normal derivate over a panel, we split the integrand into a regular and a singular part. The regular part is integrated by the mid-point rule or by the four-point Gaussian rule. Each term in the singular part is then treated separately. $1/r'$ and its derivatives are integrated by the Hess and Smith method. The logarithmic singularity in (C.5) is integrated by the method described in Newman and Sclavounos (1987). The remaining singular terms to be treated are then those involving the derivatives of the logarithmic singularity, given by (C.5). Note that we can write

$$\begin{aligned} \frac{1}{r'+|z+\zeta|} &= \left(\frac{r'}{r'+|z+\zeta|}\right)\frac{1}{r'}\\ \frac{1}{r'(r'+|z+\zeta|)} &= \left(\frac{r'}{r'+|z+\zeta|}\right)\frac{1}{r'^2}\\ &= -\left(\frac{r'}{r'+|z+\zeta|}\right)\left[\frac{x-\xi}{r'}\frac{\partial}{\partial x}\left(\frac{1}{r'}\right)+\frac{y-\eta}{r'}\frac{\partial}{\partial y}\left(\frac{1}{r'}\right)+\frac{z+\zeta}{r'}\frac{\partial}{\partial z}\left(\frac{1}{r'}\right)\right]\end{aligned} \tag{C.6}$$

From the integral equations (2.31), (2.32) and (2.34), we see that the Green function ψ_1 and its normal derivative only are integrated over the body surface, not over the free surface. From (3.14), we know that ψ_1 does not contain the Rankine source, and thus it is only singular at the free surface. We also see that the coefficients in front of $1/r'$ and

its derivatives in (C.6) always lie between 1 and -1. Thus, when the source point and the field point are close together and simultaneously close to the free surface, the expressions in (C.6) can be integrated by keeping the coefficients constant under the integration. The coefficients are then replaced with their mean values over the panel, computed by the four-point Gaussian rule. $1/r'$ and its derivatives are integrated by the Hess and Smith method.

If the source and field points are not close together or not close to the free surface, the entire forward speed Green function ψ_1 and its derivatives are integrated by the mid-point rule or by the four-point Gaussian rule.

Appendix D

The program structure

Our program is an extended version of the radiation/diffraction program WAMIT, developed at the MIT. WAMIT solves the radiation and diffraction problems at zero Froude number and computes the first-order forces and motions and the drift forces. This is documented in Newman and Sclavounos (1987). The program consists of two modules. The first module, POTEN, computes the velocity potential, while the second module, FORCE, computes the forces. The subroutine structure of our extended forward-speed WAMIT program is listed below.

D.1 The structure of the POTEN module

```
C-------------------------------------------------------------------
C     The subroutine calls made in POTEN are listed below. Indented
C     subroutine names indicate calls made by leading subroutine name
C
C     Subroutine  Source-code  Description
C        name        file
C     -------------------------------------------------------------
C     CHECK              Checks input parameters
C     GEOM               Sets-up panel geometrical data
C                        for the body surface
C       PANEL            Evaluates data for given panel
C     GEOMSF             Sets-up panel geometrical data
C                        for the free surface
C       PANEL            Evaluates data for given panel
C     MODE               Sets-up mode symmetry indices
C     POPEN              Opens files
C     SAVINP             Saves input data for use with FORCE
C     CHI                Computes derivatives of steady potential
```

```
C       MATSTD          Sets-up Rankine influence matrix
C                       for the steady problem
C         INTSTD        Computes source and dipole integrals
C           QUADR
C           RIGIDG      Computes the 1/r + 1/r' Green function
C       DBINIT          Initializes double-body matrix
C       DBSOLV          Solves double-body problem
C         SGECO         LINPACK Gauss reduction
C         SGESL         LINPACK back substitution
C       FSFCHI          Computes derivatives at the free surface
C         INTSTD
C       NMAST           Computes derivatives on the body
C         INTSTD
C     RANKIN            Sets-up Rankine influence matrix
C       REFL            Reflects field points wrt symmetry planes
C       QUADR           Computes coordinate transformations
C         RLPAN         Evaluates Rankine influence coefficients
C     SAVRNK            Saves Rankine matrix
C     RETRNK            Retrieves Rankine matrix
C     INITLS            Initializes solution matrix
C     WAVEGR            Sets-up solution matrix
C       REFL            Reflects field points wrt symmetry planes
C       FGREEN          Evaluates wave source potential
C     ROOT              Determines real root in dispersion relat.
C     DIFRHS            Sets-up RHS of diffraction problem
C       INCPOT          Evaluates incident-wave potential
C     SOLVE             Solves linear systems by Gauss reduction
C       CGECO           LINPACK complex Gauss reduction
C       CGESL           LINPACK complex back substitution
C     SAVRAD            Saves solution radiation potentials
C     SAVDIF            Saves solution diffraction potentials
C         QUADR
C         FGREEN
C     PHIDSF            Computes the zero-speed potential at the
C                       free surface
C       GREEN           Integrates G and dG/dn over a panel
C         QUADR
C         FGREEN
C     SAVFSF            Saves quantities at the free surface
C     TAUINI            Initializes forward-speed potentials
C     BODINT            Computes integral over the body of
C                       phi0dG1/dn
C       GREENS          Computes the gradient of the Green function
C                       wrt source point
```

```
C       INTDG1          Computes the integral of dG1/dn over a panel
C         QUADR
C         REGPAR        Computes the regular part of dG1/dn
C           FGREEN
C     INTF                Computes integral over the free
C                         surface of the steady disturbance
C       INTFPAN           Computes the integral over a surface panel
C                         of the gradient terms
C         QUADR
C         FGREEN
C       INTFZZ            Computes the integral over a surface panel
C                         of the second derivative terms
C         QUADR
C         FGREEN
C     F1SOLV              Solves the phi1 problem
C       CGESL             LINPACK complex back substitution
C     SAVRAD              Saves the speed-dependent radiation potential
C     SAVDIF              Saves the speed-dependent diffraction potential
C     VELINI              Initializes the velocity on the body
C     SRCMAT              Sets-up equation system for zero-speed source
C                         density
C       GREEN
C     SOLVE
C       CGECO
C       CGESL
C     SRCVEL              Computes zero-speed unsteady velocity on the body
C     SAVVEL              Saves the unsteady velocity to binary file
C     PCLOSE              Closes files
C-------------------------------------------------------------------------
```

D.2 The structure of the FORCE module

```
C-------------------------------------------------------------------------
C     The subroutine calls made in FORCE are listed below. Indented
C     subroutine names indicate calls made by leading subroutine name
C
C
C     Subroutine  Source-code  Description
C        name        file
C     ---------------------------------------------------------------------
C     CHECKF       FORCE       Checks input parameters
C     ROOT         KERNEL      Solves for real root of dispersion relat.
C     ADMDMP       FORCE       Evaluates hydrodynamic coefficients
```

C	HASKND	FORCE	Evaluates Haskind exciting forces
C	INCWAVE	FORCE	Evaluates inc. potential & normal deriv.
C	EXCFRC	FORCE	Evaluates diffraction exciting forces
C	TRNSFR	FORCE	Evaluates body motions
C	CGECG	LINPACK	Carries out complex Gauss reduction
C	CGESL	LINPACK	Complex back substitution
C	BPRESS	FORCE	Evaluates hydrodynamic pressure on body
C	FPRESS	FORCE	Evaluates pressure in fluid domain
C	INCPOT	KERNEL	Evaluates incident potential
C	REFL	KERNEL	Reflects field points wrt symmetry planes
C	GREEN	FORCE	Evaluates field potential and velocity
C	FVEL	FORCE	Evaluates velocity in fluid domain
C	INCPOT	KERNEL	Evaluates incident potential
C	REFL	KERNEL	Reflects field points wrt symmetry planes
C	GREEN	FORCE	Evaluates field potential and velocity
C	GREEN	FORCE	Evaluates field potential and velocity
C	QUADR	KERNEL	Evaluates panel coordinate transformation
C	RLPAN	KERNEL	Evaluates Rankine integrals over a panel
C	FGREEN	FINGREEN	Evaluates wave source potential
C	NNDRFT	FORCE	Evaluates surge, sway & yaw drift forces
C	KOCHIN	FORCE	Sets-up Kochin functions for drift forces
C	INCWAVE	FORCE	Evaluates inc. potential & normal deriv.
C	RETINP	FORCEIO	Retrieves input and geometry data
C	FOPEN		Opens files
C	RETRAD	FORCEIO	Retrieves solution radiation potentials
C	RETDIF	FORCEIO	Retrieves solution diffraction potentials
C	OPNRAD	FORCEIO	Run header
C	OPPER	FORCEIO	Outputs wave period
C	OPCOEF	FORCEIO	Header for hydrodynamic coefficients
C	OPHASK	FORCEIO	Header for Haskind exciting forces
C	OPXFRC	FORCEIO	Header for diffraction exciting force
C	OPTRNS	FORCEIO	Header for body motions
C	OPBPRS	FORCEIO	Header for body pressure
C	OPFPRS	FORCEIO	Header for field pressure
C	OPFVEL	FORCEIO	Header for field velocity
C	OPDRFT	FORCEIO	Header for drift forces
C	OPTAU		Header for reduced frequency
C	OPDFOR		Header for forward-speed drift force
C	PHIADD		Adds zero and first order velocity
C			potentials
C	AIJBIJ		Computes speed-dependent added mass
C			and damping
C	HASKIN		Computes speed-dependent exciting force
C			from far-field Haskind relations

```
C       FAMPR2              Computes the amplitude distribution of
C                           the radiation potentials
C     EXCIT                 Computes speed-dependent exciting force
C     FORCEX                Computes the drift force with forward
C                           speed from momentum equation
C       FAMPD2              Computes the amplitude distribution of
C                           the scattering potential
C     FORCEX2               Computes the drift force with forward
C                           speed from momentum/energy equation
C       FAMPD2              Computes the amplitude distribution of
C                           the scattering potential
C     ENFLUX2               Checks energy conservation
C       FAMPD2              Computes the amplitude distribution of
C                           the scattering potential
C     FFDAMP                Compute speed-dependent damping from
C                           energy flux in the far-field
C       FAMPR2              Computes the amplitude distribution of
C                           the radiation potentials
C     TRANSF                Computes body motions, using far-field
C                           Haskind exciting forces
C     DFORCX                Computes drift force with forward speed
C                           for a freely floating body
C     FCLOSE                Closes files
C-------------------------------------------------------------------
```